TRC-2017-02
October 31, 2018

Development of a Bicycle Dynamic Model and Riding Environment for Evaluating Roadway Features for Safe Cycling

FINAL REPORT

Upul Attanayake, Ph.D., P.E.

Mitchel Keil, Ph.D., P.E.

Abul Fazal Mazumder, M.Sc.

Transportation Research Center for Livable Communities
Western Michigan University

Technical Report
Documentation Page

1. Report No. TRCLC 2017-02	**2. Government Accession No.** N/A	**3. Recipient's Catalog No.** N/A
4. Title and Subtitle Development of a Bicycle Dynamic Model and Riding Environment for Evaluating Roadway Features for Safe Cycling		**5. Report Date** October 31, 2018 **6. Performing Organization Code** N/A
7. Author(s) Upul Attanayake, Ph.D., P.E. Mitchel Keil, Ph.D., P.E. Abul Fazal Mazumder, M.Sc.		**8. Performing Org. Report No.** N/A
9. Performing Organization Name and Address Western Michigan University 1903 West Michigan Avenue Kalamazoo, MI 49008		**10. Work Unit No. (TRAIS)** N/A **11. Contract No.** TRC 2017-02
12. Sponsoring Agency Name and Address Transportation Research Center for Livable Communities (TRCLC) 1903 W. Michigan Ave., Kalamazoo, MI 49008-5316 USA		**13. Type of Report & Period Covered** Final Report 8/15/2017 - 10/31/2018 **14. Sponsoring Agency Code** N/A
15. Supplementary Notes		

16. Abstract

Cycling is a viable transportation option for almost everyone and enhances health, equity, and quality of life. Cycling contributes to the society by reducing fuel consumption, traffic congestion, and air and noise pollution. In recent days, cycling has been promoted as more emphasis is given to non-motorized mobility. To attract people towards cycling, safe and comfortable bikeways are needed. The impact of bikeway design parameters on bicycle stability (safety) and rider comfort can be evaluated using simulation models. Therefore, a dynamic simulation model is developed in ADAMS using the Whipple benchmark bicycle model parameters. Vertical equilibrium, theoretical centripetal acceleration, and experimental data collected using an instrumented probe bicycle (IPB) are used to validate the model. The bicycle model is simulated over a predefined horizontally curved bikeway at different velocities to calculate slip angle, centripetal acceleration and jerk. The results show that the slip angle, centripetal acceleration and jerk increase with the increase of bicycle velocity and degree of curvature. Depending on the available transition curves, a significant jerk could be generated at the entrance and exit of a curve. As the outcome of this research, a graphical tool is presented that can be used to determine the upper limit of the velocity for a given horizontal curve to limit the jerk. Alternatively, this tool can be used to determine the jerk in order to design transition curves for a given horizontal curve and a selected velocity.

17. Key Words ADAMS, Bicycle, Ride comfort, Safety, Transition curve	**18. Distribution Statement** No restrictions.

19. Security Classification - report Unclassified	**20. Security Classification - page** Unclassified	**21. No. of Pages** 72	**22. Price** N/A

DISCLAIMER

ACKNOWLEDGMENTS

This research was funded by the United States Department of Transportation (USDOT) through the Transportation Research Center for Livable Communities (TRC-LC), a Tier 1 University Transportation Center. Authors would like to thank TRC-LC at Western Michigan University for funding this study through the University Transportation Center's (UTC) program.

TABLE OF CONTENTS

LIST OF TABLES

TABLE OF FIGURES

1 INTRODUCTION

1.1 OVERVIEW

Cycling is regarded as a very effective and efficient mode of transportation for short and moderate distances. Cycling is a viable transportation option for almost everyone and contributes to the health, equity, and quality of life. Cycling reduces fuel consumption, traffic congestion, and air and noise pollution. In 2017, approximately 66.21 million people used bicycles in the United States of America (USA) (Statista 2018). Recently, cycling has been promoted as more emphasis is given to non-motorized mobility (Smart Growth America 2013). In order to attract more people towards cycling, safe and comfortable bikeways are needed.

A bikeway facility is designed following the guidelines published by the American Association of State Highway and Transportation Officials (AASHTO) and other highway agencies. AASHTO (2011) and the California Highway Design Manual (Caltrans HDM 2016) define four classes of bikeways: bike path, bike lane, bike route, and shared roadway. Four sub-classes of bike lanes are the conventional bike lane, the buffered bike lane, the contra-flow bike lane, and the left-side bike lane (NACTO 2018). Figure 1-1 shows classes and sub-classes of bikeways. Even though these manuals provide minimum requirements of bikeway geometric design parameters to enhance safety, bikeway geometric parameters are primarily controlled by the existing roadway features that can influence bicycle stability and rider comfort. Design engineers have more flexibility when designing a bike path than any other bikeways since a bike path is separated from the existing roadway.

Static and dynamic comfort is enhanced to improve safety and ride comfort (Cervélo 2015). Manufacturers are constantly working to enhance static and dynamic comfort by improving bicycle and outfit design (Cycling Weekly 2018). A vertical excitation develops due to bikeway surface texture and vertical profile and results in a vibration that transmits to the hands and buttocks. Naturally, this vibration is a significant source of discomfort. As an example, a small bump can transmit about 1.5W to 4W to a rider's hands and buttocks (Wikstrom 2016). Moreover, centripetal acceleration acts on a cyclist when travelling along a curve. The rate of change of centripetal acceleration results in a jerk that causes discomfort to the cyclist. With a significant jerk, a cyclist tends to lose control of a bicycle. Hence, transition curves are provided at the beginning and end of a curve to control the rate of change of centripetal acceleration.

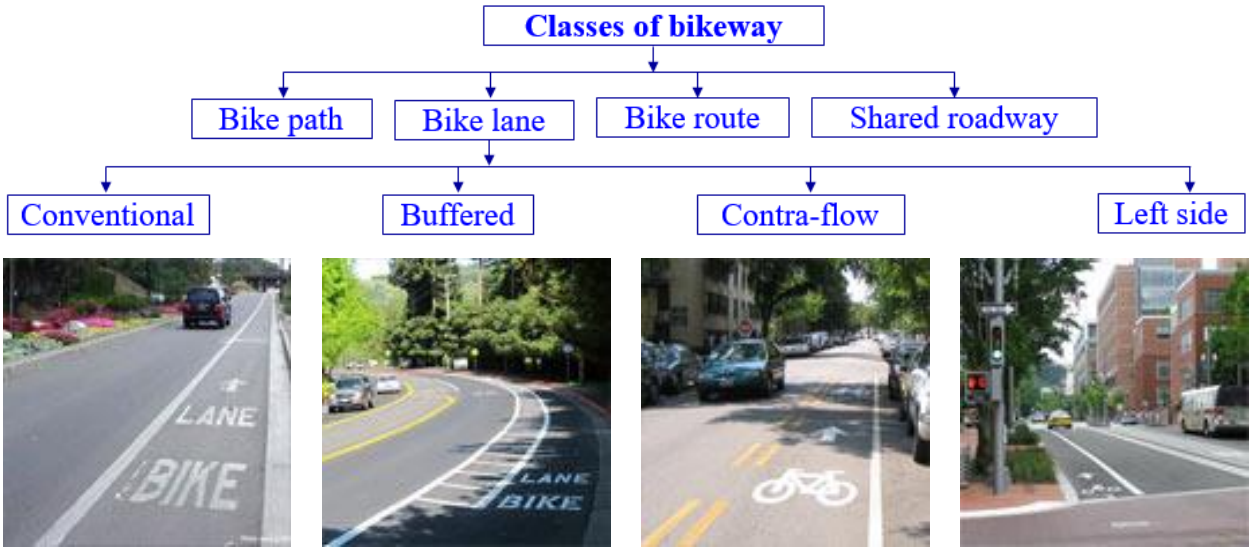

Figure 1-1. Classes of bikeway

Besides static and dynamic comfort, bicycle stability is a safety concern. A bicycle is self-stable within a certain velocity range (Meijaard et al. 2007). When a bicycle is not in a self-stable position, the rider's input is needed to make it stable. A Rider's input includes force and torque provided through a handlebar to control and guide a bicycle, leaning the bicycle while negotiating a horizontal curve, and offering power output to control velocity.

Researchers, bicycle manufacturers, and other agencies work together to increase safety and ride comfort. Various research methods and techniques are used for such studies. A few examples are the use of verbal/written surveys, video recording, GPS devices and smartphones, instrumented bicycles, and virtual reality technologies. These methods are indispensable to evaluate human response and impact of bikeway design parameters. Also, simulation models can be used to evaluate the impact of several bikeway design parameters on bicycle stability (safety) and rider comfort. The major advantages of using simulation models include (i) keeping people off the road during evaluation, (ii) creating the opportunity to evaluate the impact of specific parameters uncoupled from the other parameters that are typically hard to separate in an experimental setup, (iii) using as a tool for experimental design, and (iv) offering the potential to evaluate the impact of design parameters before implementation.

1.2 OBJECTIVE AND SCOPE

The primary objective is to develop a bicycle dynamic model and riding environment for evaluating the impact of bikeway design parameters on stability and rider comfort.

To accomplish the aforementioned objective, the following four tasks are developed:

a) Perform a state-of-the-art and practice review on bikeway design, bicycle models and simulation efforts, along with stability and rider comfort evaluation.

b) Develop and validate a simulation model in the ADAMS environment.

c) Evaluate the impact of bikeway design parameters on stability and rider comfort.

d) Develop recommendations and deliverables.

The scope of this study is limited to developing a simulation model, validating the model with fundamentals and experimental data collected using an instrumented probe bicycle, and performing simulations to evaluate the impact of bikeway design parameters on stability and rider comfort.

1.3 REPORT ORGANIZATION

The report is organized into 6 chapters:

- Chapter 1 includes an overview, objective and scope.
- Chapter 2 provides a review of state-of-the-art and practice related to improving safety and ride comfort. The chapter includes classes of bikeway and minimum design requirements of their components, typical components of a bicycle, forces acting on a bicycle while travelling on a horizontal curve, design considerations of a transition curve, ride comfort due to surface texture and vertical profile, and modeling and simulation efforts.
- Chapter 3 documents benchmark bicycle model parameters and development and validation of a simulation model.
- Chapter 4 documents evaluation results of bikeway design parameters.
- Chapter 5 provides a summary, conclusions, and recommendations.
- Chapter 6 includes the list of references.

The report appendices include the following:

- Appendix A: Abbreviations
- Appendix B: Coefficients of linearized equations
- Appendix C: MATLAB code

2 STATE-OF-THE-ART AND PRACTICE REVIEW

2.1 OVERVIEW

AASHTO (2011) and Caltrans HDM (2016) define four classes of bikeways: bike path, bike lane, bike route, and shared roadway (Figure 1-1). A bike lane is further classified in to 4 sub-classes: conventional bike lane, buffered bike lane, contra-flow bike lane, and left-side bike lane (NACTO 2018). Table 2-1 and Table 2-2 present the definition of classes and sub-classes of bikeways, respectively. Manuals and guides provide the minimum recommendations for bikeway design parameters. This chapter presents a summary of the design parameters and the minimum recommendations.

Safety is evaluated by considering the potential for collision of cyclists with motorized vehicles, pedestrians, or other bikeway features. A significant amount of research has been conducted in that area, and guidelines and tools for such evaluations are presented. As an example, the Ireland National Transport Authority presents a guidance graph in their National Cycle Manual (NCM 2011) for the selection of shared lane, bike lane, or a bikeway based on the traffic volume and motorized vehicle speed (Figure 2-1). As shown in the figure, a shared lane is preferred when the average annual daily traffic (AADT) is less than 2000 and the posted motorized vehicle speed is less than 20 mph. Whereas, a bike path is the only choice when the AADT is greater than 10,000 or the vehicle speed is greater than 40 mph. Another aspect of safety evaluation is the evaluation of bicycle stability, the focus of this study. Cain and Perkins (2010), Cheng et al. (2003), Åström et al. (2005), and Lorenzo (1997) used an instrumented bicycle to measure the required steering torque to control a bicycle while travelling uphill, downhill, and around a steady turn and a sharp turn. Another approach can be the use of simulation tools to evaluate the impact of bikeway features on stability. Such efforts are summarized in this chapter where the relevant information is available.

Comfort is evaluated by considering the cyclists' feelings and response when travelling along with the motorized vehicles or on narrow lanes/paths. A significant number of studies have been conducted in that aspect. As an example, video recording and virtual reality are used to evaluate cyclists and motorized vehicle response to recommend bikeway design parameters (De Leeuw and De Kruijf 2015). The guidance graph presented in NCM (2011) also considers a cyclist's comfort when selecting bikeways along various roadways. As shown in Figure 2-1, posted

motorized vehicle speed and traffic volume are two main parameters used to define the level of comfort that a cyclist feels when travelling with the motorized vehicles. Cyclists feel very comfortable using shared lanes when the volume of traffic is low and the posted speed is less than 20 mph. However, as the posted speed increases to more than 40 mph, use of a separate bike path is required to make cyclists feel safe.

Comfort is also evaluated in terms of ride quality. Li et al. (2013) developed a survey to evaluate ride quality. According to CYCLINGTIPS (2018) and Lépine et al. (2013), cyclists' response due to vertical excitation is monitored to improve bicycle design and ride quality. Another approach can be the use of simulation tools to evaluate the impact of bikeway features on jerk and the effort need by a cyclist to negotiate a curve – the focus of this study as the cyclist's comfort. Developing a bicycle simulation model requires a thorough understanding of its components and material, forces developed on the bicycle while travelling along a curved path, and the rider's contribution to control the stability and velocity of a bicycle. This chapter presents bicycle modeling related information and the efforts by various researchers to evaluate ride comfort.

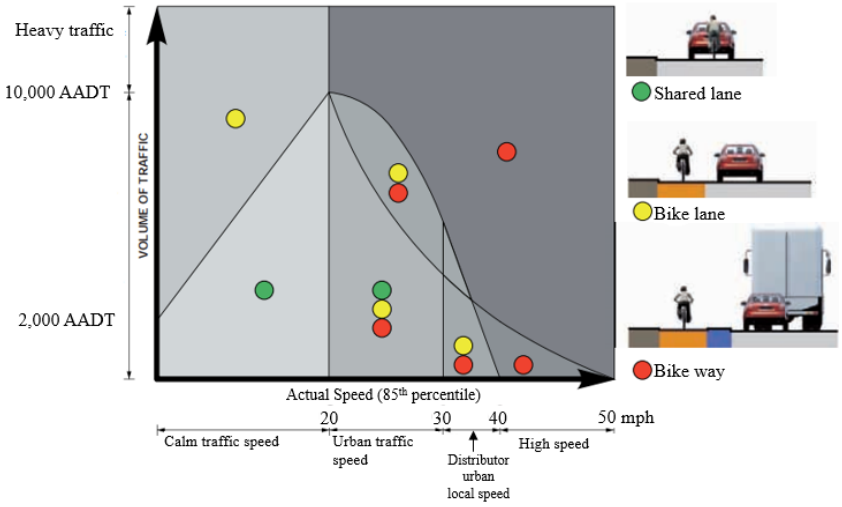

Figure 2-1. Guidance graph (NCM 2011)

2.2 BIKEWAY DESIGN PARAMETERS

The following is a list of typical bikeway design parameters:

a) Separation width between a bikeway and roadway
b) Design speed
c) Horizontal curvature
d) Superelevation
e) Grade and cross slope
f) Sight distance
g) Stopping sight distance
h) Sight distance at horizontal curve
i) Width of bikeway
j) Horizontal and vertical clearance
k) Friction

To ensure safety, manuals and guides provide the minimum required design values of these parameters (Attanayake et al. 2017). A summary is presented in Table 2-3.

Table 2-1. Classes of Bikeway with Definition (Caltran HDM 2016)

Class of bike ways	Definition
Class I (bike path)	A bicycle facility that is separated from motorized vehicular traffic
Class II (bike lane)	A lane designated for exclusive or preferential use by bicycles through the application of pavement striping or markings and signage
Class III (bike route)	A roadway designated for bicycle use through the installation of directional and informational signage
Class IV (shared roadway)	A roadway where cyclists share a traffic lane with motorized traffic

Table 2-2. Different Types of Bike Lanes (NACTO 2018)

Types of bike lane	Definition
Conventional bike lane	A bicycle lane located adjacent to motor vehicle travel lanes and which flows in the same direction as motor vehicle traffic
Buffered bike lane	A conventional bike lane with a designated buffer space separating the bicycle lane from the adjacent motor vehicle travel lane and/or parking lane
Contra-flow bike lane	A bicycle lane designed to allow bicyclists to ride in the opposite direction of motor vehicle traffic
Left side bike lane	A conventional bike lane placed on the left side of one-way streets or two-way median divided streets

Table 2-3. The Minimum Requirements of Bikeway Design Parameters

Design elements				**Criteria**
Width of bikeway	Class I (Bike paths)	Two-way		Min. 8 ft is preferred 10 ft or 12 ft for heavy cyclist volume
		One-way		Min. 5 ft
		Bike path on structure (bridge and overpass)		Min. 10 ft
	Class II (Bike lanes)	Curbed streets without parking	Two-way curb and gutter section (one-way bike lane)	Min. 4 ft
			Two-way monolithic curb and gutter section (one-way bike lane)	Min. 5 ft
		Curbed streets with parking	Unmarked bike lane	Min. 13 ft
			Marked bike lane	Min. 5 ft, parking 8 ft
		Bicycle lanes adjacent to bus lanes		Min. 5 ft
		One-way bike lane on shoulder		Min. 4 - 6 ft
		One-way bike lane on roadway		Min. 4 ft
		One-way bike lane cross a structure like bridge		Min. 5 ft
		Shared lane on roadway		Min. 13 - 14 ft
	Class III (Bike route)			Minimum standards for highway lanes and shoulder
	Class IV (Shared roadway)			4 ft of paved roadway shoulder with 4 in. edge line
Cross slope				Max. 2%, Min. 1%
Shoulder width				Min. 2 ft (preferable 3 ft) with slope 2 - 5%
Shy distance				Min. 2 ft on each side
Separation width from pedestrian walkway				Min. 5 ft
Clear distance to obstruction from bike path			Horizontally	Min. 2 ft (preferable 3 ft)
			Vertically	Min. 8 ft across width and 7 ft over shoulder
Ramp width				Same width of bicycle path with smooth transition between bicycle path and the roadway
Paving width at crossings of roadway or driveway				Min. 15 ft
Separation width of bike paths parallel & adjacent to streets and highway				Min. 5 ft plus shoulder width.
Posted speed limit		Mopeds prohibited bike paths		20 mph
		Mopeds permitted bike paths		30 mph
		Bike paths on long downgrades (steeper than 4% and longer than 500 ft)		30 mph

Table 2-3. The Minimum Requirements of Bikeway Design Parameters (contd.)

Superelevation rate		Max. 2%
Horizontal Alignment	Radius of curvature with Superelevation rate	90 ft for 20 mph 160 ft for 25 mph 260 ft for 30 mph.
	Radius of curvature without Superelevation rate	100 ft for 20 mph 180 ft for 25 mph 320 ft for 30 mph.
Stopping sight distance		Min. 125 ft for 20 mph Min. 175 ft for 25 mph Min. 230 ft for 30 mph.
Length of transition curve		Min 25 ft for 3% superelevation
Grades		Min. 2%, Max. 5 %
Length of the crest of vertical curves		$L = 2S - \frac{1600}{A}$ when S > L $L = \frac{AS^2}{1600}$ when S < L where, L is minimum length of vertical curve in feet S is stopping distance in feet A is algebric grade difference
Lateral clearance on horizontal curves		$m = R\left[1 - \cos\left(\frac{28.65S}{R}\right)\right]$ where, m is minimum lateral clearance in feet S is stopping distance in feet R is radius of center of lane in feet
Lighting		Average illumination of 5 - 22 lux
Speed bumps, gates, obstacles, posts, fences, or other similar features intended to cause bicyclists to slow down		Not required
Entry control for bicycle paths		Required
Signing and delineation		MUTCD section 9B and 9C

Sources:
1. Caltran HDM (2016)
2. BDE Manual (2016)
3. MnDOT (2007)

2.3 BICYCLE - COMPONENTS, GEOMETRY, AND MATERIAL

Static and dynamic comfort depends on bicycle components, geometries, and material. Components of a typical bicycle are shown in Figure 2-2. Static comfort depends on several design parameters of a bicycle at rest. The following parameters typically contribute to the static comfort: handlebar height, saddle height and angle, reach (distance between saddle point and gripping point of the handlebar), cleat positioning of a rider, and a rider's outfit (Cycling Weekly 2018).

Dynamic comfort refers to the feeling of a rider on a moving bicycle. Similar to static comfort, several bicycle design parameters and a rider's outfit affect the dynamic comfort (Cervélo 2015). Bicycle manufacturers work in collaboration with researchers to evaluate the dynamic comfort by conducting laboratory experiments (CYCLINGTIPS 2018). The VÉLUS laboratory conducts extensive studies on dynamic comfort of road bicycles (VÉLUS 2018). Figure 2-3b shows one of the laboratory experimental setups used by this group. Evaluation of dynamic comfort is very complex. A survey conducted by the VÉLUS group has identified the saddle design as one of the most critical features to improve dynamic comfort. As a prominent group in bicycle research, laboratory and field experiments have been conducted to understand and evaluate ride quality. In addition to conducting experimental studies, the use of high-fidelity simulation models could help refine the experimental design by performing a large number of evaluations.

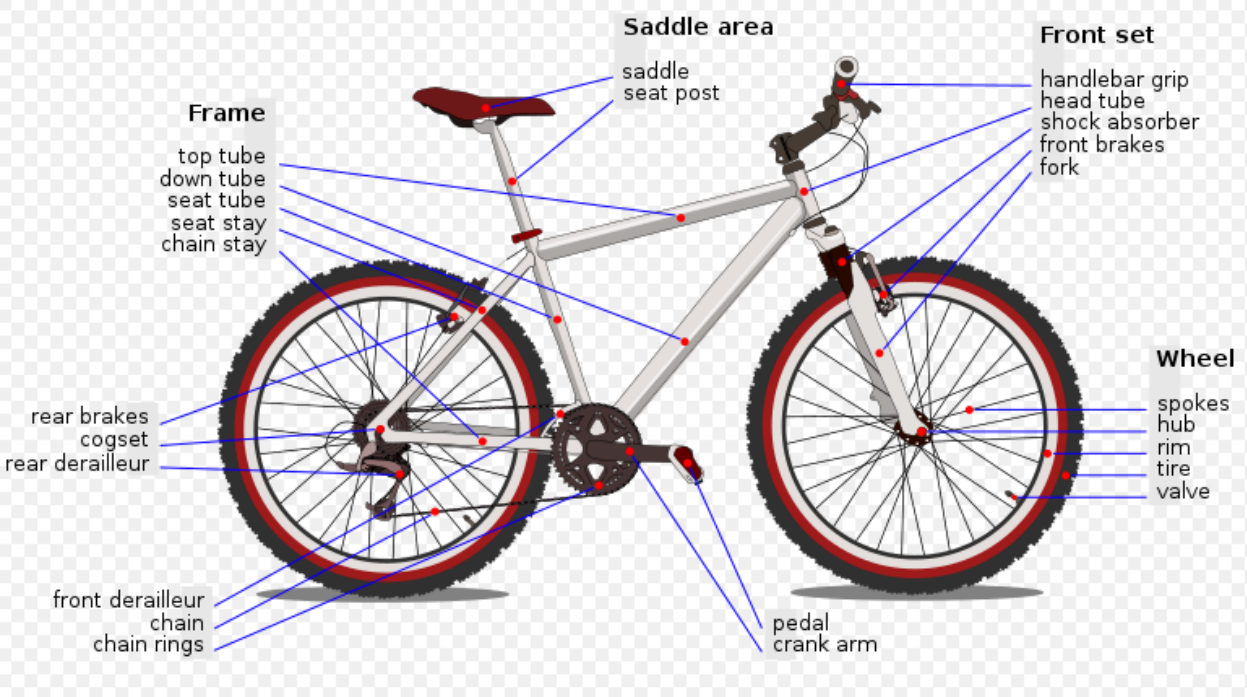

Figure 2-2. Components of a typical bicycle (Wikipedia 2018)

a) Vertical excitation on front wheel test on a treadmill (CYCLETIPS 2018)

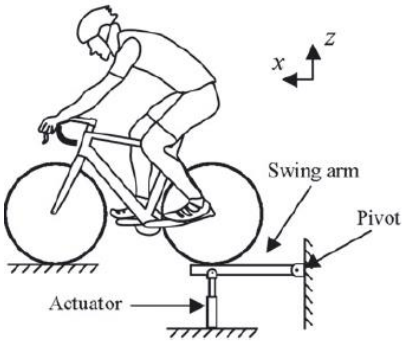

b) Vertical excitation on rear wheel test using actuator (Lépine et al. 2013)

Figure 2-3. Test setup for evaluating dynamic comfort due to vertical excitation

2.3.1 Frame

The frame is the main component of a bicycle. Wheels and other components are fitted onto the frame. A typical bicycle frame is known as a diamond frame, which consists of two triangles – a main triangle and a paired rear triangle. Figure 2-4 shows a diamond frame. The main triangle consists of the head tube, top tube, down tube, and seat tube. The rear triangle consists of the seat tube, paired chain stays, and seat stays. The frame is manufactured with different material for different kinds of bicycles. As an example, the superlight frame for a racing bicycle is

manufactured using carbon fibers to increase the speed and shock absorbing capacity. The most commonly used frame materials are AISI 1020 steel, aluminum alloys, Titanium alloys, carbon fiber reinforced polymer (CFRP), Kevlar fiber reinforced polymer (KFRP), glass fiber reinforced polymer (GFRP), and wood or bamboo. The application of such materials depends on the cost and intended use of a cycle. Maleque and Dyuti (2010) developed an algorithm to select optimum material for a bicycle using the cost per unit strength method and a digital logic model depending on general material performance requirements. The performance requirements are density, stiffness, yield strength, elongation, fatigue strength, and toughness.

Figure 2-4. Diamond frame of a bicycle with fork

2.3.2 Wheel

The fundamental purpose of a wheel is to provide smooth rolling of a bicycle. The most common components of a wheel are a hub, spokes, a rim, a tire, and a tube. Currently, cycle manufacturing companies are making the wheel tubeless. Each part of the wheel requires different material. Table 2-4 shows wheels components and commonly used manufacturing materials.

Table 2-4. Wheels Components and Manufacturing Material

Wheel component	Manufacturing material
Hub	Steel
Spoke	Steel
Rim	Steel and iron alloyed with other material
Tire	Rubber
Tube	Rubber

2.3.3 Tire Pressure

The required tire pressure for ride comfort depends on the intended use and the weight of the rider as shown in Table 2-5.

Table 2-5. Required Tire Pressure for Intended Use and Rider's Weight (Bicycling 2018)

Intended use and required tire pressure		**Weight of the rider and required tire pressure**	
Use	Tire pressure (psi)	Weight of the rider (lbs)	Tire pressure (psi)
Road tires	80 – 130	130	80
Mountain tires	25 - 35	165	100
Hybrid tires	50 - 70	200	120

2.3.4 Position of the Saddle

Perfect positioning of a saddle is very important for both static and dynamic comforts. A high saddle may cause iliotibial (IT) band syndrome. Fifteen percent (15%) of all cyclists' knee pain is caused by IT band syndrome. A low saddle is less likely to cause an injury, but it compromises pedaling efficiency. For a good saddle height, it is recommended to set the distance between the top of the saddle to the middle of the lower bracket equals to the length of the rider's inside leg height minus 3.93 in. (10 cm) (Cycling Weekly 2018).

2.3.5 Suspension

Suspensions are used to control the vibration and force transmission to the rider. Suspensions are primarily used in mountain bicycles. However, they are also used in hybrid and ordinary bicycles. Suspensions are mounted at several locations on a bicycle: front fork, stem, seat post, rear, and any combination thereof. Besides providing comfort to the rider, suspensions improve both efficiency and safety while maintaining one or both wheels in contact with ground and allowing the rider's mass to move over the ground smoothly (Cycle Weekly 2018).

2.4 FORCES ACTING ON A BICYCLE

A bicycle travelling along a horizontal curve is subjected to several forces: i) a reaction normal to the road and tire contact surface, ii) a frictional force, iii) a vertical force due to gravitational acceleration and the weight of the bicycle and the rider, and iv) a centrifugal force. The centripetal acceleration (a_c) for a point-mass travelling at a constant speed (V) along a horizontal curve of a constant radius (R) equals to V^2/R. The centripetal acceleration is a constant for a given constant velocity and radius.

As shown in Figure 2-5a, a bicycle travelling along a horizontal curve maintains its equilibrium by leaning towards the center of the curve. The lean angle is θ. The resultant force (F) of normal reaction (N) and frictional force (F_f) is acting towards the center of gravity. Since all three forces (F, W = mg, and centrifugal force $F_c = \frac{mV^2}{R}$) pass through the center of gravity, a force triangle can be drawn to represent the equilibrium (stability) of the bicycle, as shown in Figure 2-5b and Figure 2-5c. After considering vertical and horizontal force equilibrium, the lean angle can be represented using Eq. 2-1.

$$\theta = \tan^{-1}\frac{V^2}{gR} \qquad (2\text{-}1)$$

For a gravitational acceleration of 32.2 ft/s^2, speed in miles per hour, and a radius in ft, the lean angle in degree (º) can be calculated using Eq. 2-2.

$$\theta = \tan^{-1}\frac{0.067V^2}{R} \qquad (2\text{-}2)$$

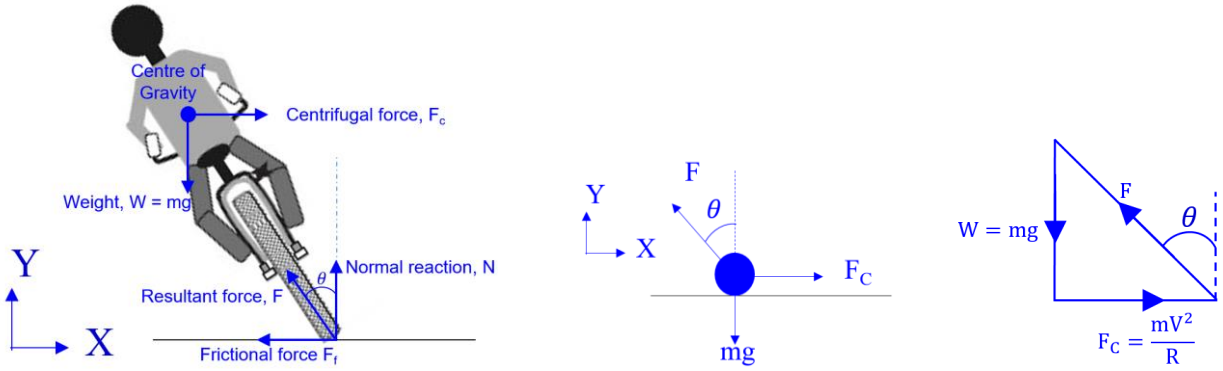

a) Forces acting on a bicycle when travelling along a horizontal curve

b) Resultant forces acting through the center of gravity

c) Force triangle

Figure 2-5. Forces acting on a bicycle while travelling along a horizontal curve

The allowable lean angle used for design is 15º while the maximum angle is 20º for an average cyclist. The bicycle pedal could touch the ground at 25º (MnDOT 2007). As shown in Table 2-6, Eq. 2-2 can be used to calculate the minimum radius of a horizontal curve for different posted speed limits and allowable and maximum lean angles.

Table 2-6. Minimum Radius of Horizontal Curve for 15º and 20º Lean Angle (MnDOT 2007)

Posted speed limit, V (mph)	Minimum radius, R (ft)	
	Lean angle (θ) = 15º	Lean angle (θ) = 20º
12	36	27
20	100	74
25	156	115
30	225	166

When a superelevation is provided to enhance bicycle stability, the forces shown in Figure 2-6 are developed as a bicycle travels along a horizontal curve. When the rate of superelevation (e) is expressed as a percentage, the banking angle as α, and the coefficient of side friction as f, Eq. 2-3 can be derived by considering the equilibrium of the bicycle to calculate the centripetal acceleration.

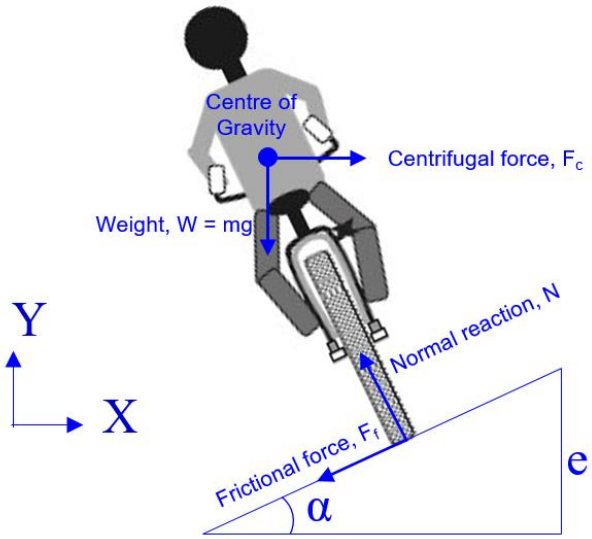

Figure 2-6. Forces acting on a bicycle travelling along a horizontal with a superelevation

$$\frac{g\left(f+\frac{e}{100}\right)}{1-f\frac{e}{100}} = \frac{V^2}{R} \qquad (2\text{-}3)$$

Since the f and e are too small, the denominator of the left-hand side of Equation 2-3 can be regarded as 1. With such assumptions, Eq. 2-4 can be used to calculate R for a given e, f, and V.

$$R = \frac{V^2}{g\left(f+\frac{e}{100}\right)} \qquad (2\text{-}4)$$

For a gravitational acceleration of 32.2 ft/s^2, speed in miles per hour, and the rate of superelevation in percentage, R in ft can be calculated using Eq. 2-5.

$$R = \frac{V^2}{15\left(f+\frac{e}{100}\right)} \qquad (2\text{-}5)$$

MnDOT (2007) provides the minimum radius of a horizontal curve for different posted bicycle speed limits, 2% superelevation, and a different coefficient of side friction (Table 2-7).

Table 2-7. Minimum Radius of a Horizontal Curve with 2% Superelevation (MnDOT 2007)

Posted speed limit, V (mph)	Coefficient of side friction, f	Minimum radius, R (ft)
12	0.31	30
16	0.29	55
20	0.28	90
25	0.25	155
30	0.21	260

2.5 TRANSITION CURVE

Centripetal acceleration, thus a centripetal force, develops on an object travelling along a curve. Centripetal acceleration is defined as V^2/R, where V is the velocity in the tangential direction and R is the radius of the curve. Hence, the centripetal acceleration changes with the change in velocity, radius, or a combination thereof. The rate of change of acceleration is defined as jerk. Even if a bicycle travels at a constant velocity, a jerk results due to the change in radius. Hence, a jerk is expected at the entrance and exit of a curve. The magnitude of the jerk is controlled by providing transition curves at the beginning and end of a curve to enhance the stability and level of comfort. The length of a transition curve is calculated based on the following factors:

a) the rate of change of centripetal acceleration or jerk
b) superelevation and extra widening requirements
c) an empirical equation developed by Indian Roads Congress (IRC) as a function of the centripetal acceleration (IRC 2010)

Table 2-8 lists the equations to calculate the length of a transition curve. Eq. 2-4 is a function of the centripetal acceleration and jerk (AASHTO 2011). Eq. 2-5 is an empirical formula proposed by IRC (2010) to calculate jerk as a function of the posted speed. AASHTO (2011) specifies jerk limits for highways as 1 – 3 ft/s^3 (0.3 – 0.9 m/s^3). Eq. 2-6 is a function of roadway width, extra widening required at a horizontal curve, superelevation, and longitudinal slope to apply superelevation (The Constructor 2018). Unlike for highways, a 2% maximum superelevation is specified in bikeway design manuals (MnDOT 2007). Moreover, a longitudinal slope of 1:150 is used for flat terrain (The Constructor 2018). Eq. 2-7 is the empirical equation presented in IRC (2010).

Table 2-8. Equations and Parameters to Calculate the Length of a Transition Curve

Rate of change of centripetal acceleration	Rate of change of superelevation and extra widening	IRC[1] empirical formula
$L_s = \frac{3.15\ V^3}{CR}$ (2-4) $C^1 = \frac{80}{75+1.61\ V}$ (2-5) L_s is length of a transition curve (ft) V is posted speed limit (mph) R is radius of a horizontal curve (ft) C is jerk (ft/s^3)	$L_s = (W + W_e)\ e\ N$ (2-6) L_s is length of a transition curve (ft) W is width of bikeway (ft) W_e is extra widening of bikeway in horizontal curve (ft) e is rate of superelevation (%) N is longitudinal slope to apply superelevation	$L_s = \frac{74.40\ V^2}{R}$ (2-7) L_s is length of a transition curve (ft) V is posted speed limit (mph) R is radius of a horizontal curve (ft)
1. IRC (2010)		

2.6 RIDE COMFORT

Several materials and paving schemes are used to make the riding surface smoother for improving ride comfort. Unsurfaced granular, granular with sprayed treatment, granular with bituminous slurry surfacing, granular with asphalt, hot mix asphalt pavement, concrete pavement, chip seal, concrete block paver, and paving fabrics are used for preparing bikeways (DPTI 2015, NAPA 2002, and Li et al. 2013). These materials result in different surface textures. Pavement surface texture, which is responsible for pavement roughness, is an important parameter that influences the comfort of cycling. Pavement surface texture is defined, based on the maximum dimension (wavelength) of its deviation from a true planar surface, as rough, megatexture, macrotexture, and microtexture. Vertical profile changes due to bumps, potholes, railway grade, and ramps. Ride comfort is primarily affected by megatexture (wavelengths of 0.5 mm to 50 mm) and roughness (wavelengths greater than 500 mm) (Li et al. 2013). Thigpen et al. (2015) used chip seals to improve the surface texture of a road and conducted a survey to collect cyclists' experiences while traveling over the chip-sealed road. Based on the response, a correlation of macrotexture and bicycle ride quality was developed by using multilevel statistical regression analysis models. It was found that there are strong correlations between mean profile depth, bicycle vibration, and level of ride quality. The vibration of a cycle-rider system escalates with the increase of a mean profile depth; this lowers the ride comfort. Medium to weak correlations were identified between international roughness index, bicycle vibration, and level of ride quality. Bicycle vibration escalates with the increase in the international roughness index; this lowers the ride comfort (Thigpen et al. 2015). Vibration, generated by road surface irregularities and transmitted to the rider's hands and buttocks, can be a significant source of discomfort. The

amount of power absorbed at the saddle and cockpit vary significantly for different types of vertical excitation. As an example, a small bump can transmit about 1.5W to 4W to the rider's hands and buttocks (Wikstrom 2016). According to Wikstrom (2016), wrapping a frame with damping material reduces the magnitude of certain frequencies travelling through the frameset when it was tested on its own, but this approach had no effects on vibrations when travelling with a cyclist. Bicycle manufacturers, working in collaboration with researchers, evaluate the dynamic comfort by conducting laboratory experiments (CYCLINGTIPS 2018). For example, the VÉLUS laboratory conducts extensive studies on the dynamic comfort of road bicycles (VÉLUS 2018). However, the use of high-fidelity simulation models for evaluating ride comfort is not documented.

As discussed in Section 2.5, centripetal acceleration, thus a centripetal force, develops on an object travelling along a curve. The rate of change of acceleration is defined as jerk. Depending on the significance of jerk, cyclists might feel uncomfortable riding along the path or could lose control if the jerk is significant. Even though providing transition curves at the beginning and end of a curve controls the jerk magnitude, when bikeways are established along existing roadways, it is challenging to redefine transition curves for bikeways. This requires evaluating the impact of the transition curves on the jerk, thus the comfort of the rider and stability of the bicycle.

2.7 MODELING AND SIMULATION

At present, there is an emphasis on developing autonomous (rider-less) bicycles. Hence, bicycle models are developed to perform parametric studies and to develop control systems. Limebeer and Sharp (2006) used the benchmark Whipple bicycle model to measure steer torque due to a roll angle up to 40˚ and measured torques in the realm of – 0.5 to 2.5 Nm. Sharp (2007) used the benchmark bicycle model and a Linear-Quadratic Regulator (LQR) controller to follow a randomly generated path that has about 2 m of lateral deviations. The travelling speed of the bicycle was set to 10 m/s, and the steer torque that is required to control the bicycle was measured. The steer torque was found to be – 15 to + 15 Nm. The steer torque required to control a bicycle travelling from a straight line to a circle path ranges from – 0.5 to 0.5 Nm for loose control and – 2.5 to 2.5 Nm for medium control. Meijaard et al. (2007) developed the canonical Whipple model and could make the model in SPACAR. Basu-Mandal et al. (2007)

used a non-linear approach to the Whipple model to simulate bicycle movement. Connors and Hubbard (2008) modeled a recumbent bicycle using the Whipple model and incorporated the contribution of a rider with rotating legs to study the stability at 5 – 30 m/s speed. The required steering torque to maintain bicycle stability is ±8 Nm, which is a function of the oscillation frequency of the legs. Sharp (2008) used the benchmark bicycle model and an LQR controller to measure required steer torque to perform lane changing on a 4 m wide bicycle track at 6 m/s speed. The steered toque ranged from about – 1 to + 1 Nm. According to Peterson and Hubbard (2009) less than 3 Nm steer torque is required to stabilize a bicycle due to 0 – 10˚ lean angles and a 0 to 45˚ steering angle. Jason Moore (2012) used a non-linear Whipple model and Kane's model to study the complexities of rider control. Kostich (2017) developed a bicycle model in MATLAB to simulate bicycle movement using Kane's model and validated the model with the benchmark bicycle Whipple model.

2.8 SUMMARY

AASHTO (2011) and Caltrans HDM (2016) provide a classification of bikeways. Manuals and guides provide the minimum recommendations for bikeway design parameters. Moreover, the guidance graph developed by the Ireland National Transport Authority (NCM 2011) can be used to identify and evaluate various options for accommodating bicycles along existing or planned roadways by considering safety and rider comfort. A significant amount of resources and effort has been invested in evaluating ride comfort through experimental studies that incorporate various sensors, image/video recording devices, and virtual reality technology. The main focus of such studies was to evaluate the rider comfort (i) due to road surface characteristics, (ii) when travelling with traffic and/or within a defined lane, and (iii) when encountering other obstacles and different exposure conditions. The other documented efforts are towards quantifying the torque developed due to different maneuvers of a bicycle. However, the use of high-fidelity simulation models for evaluating ride comfort and stability due to bike lane design parameters (such as radius, transition curves, speed, etc.) is not documented.

3 BICYCLE STABILITY AND MODELING

3.1 OVERVIEW

Stability and dynamic behavior of a bicycle have been studied for more than 140 years. Various mathematical models were developed and refined to better understand the bicycle response and stability, the human-bicycle interaction, and ride comfort. The evolving history of bicycle model development is well documented in Meijaard et al. (2007) and Moore (2012). The Whipple model is used as the benchmark bicycle model. The objective of this study is to develop a numerical simulation model of a bicycle in the Automatic Dynamic Analysis of Mechanical Systems (ADAMS) software. For this purpose, the Whipple model parameters were used. This chapter presents the development of the bicycle model, benchmark bicycle mathematical model, self-stable bicycle parameters of the benchmark model, development of a bicycle model in ADAMS, and model validation.

Since literature presents the bicycle model parameters and analysis results used for this research in SI units, from this point onwards, the report will use SI units to be consistent with the published research. The key results are also presented in imperial unit.

3.2 BENCHMARK BICYCLE MODEL

The benchmark bicycle model shown in Figure 3-1 consists of four parts: i) rear wheel, ii) rear frame including rider body, iii) front handlebar and fork assembly, and iv) front wheel. Papadopoulos (1987) developed the dynamic equation of motion for the benchmark bicycle model shown in Eq. 3-1. M, C_1, K_o, and K_2 represent the mass matrix, damping-like matrix, gravity-dependent stiffness matrix, and velocity-dependent stiffness matrix, respectively. The time-varying quantities are presented by q. The torque developed in the model due to steer and lean angles is represented by f. The benchmark model includes 25 design parameters as presented in Table 3-1. These parameters are used to calculate M, C_1, K_o, and K_2. The equations calculating M, C_1, K_o, and K_2 are presented in Appendix B.

$$M\ddot{q} + vC_1\dot{q} + [gK_o + v^2K_2]q = f \quad (3\text{-}1)$$

$$\det(M\lambda^2 + vC_1\lambda + gK_o + v^2K_2) = 0 \quad (3\text{-}2)$$

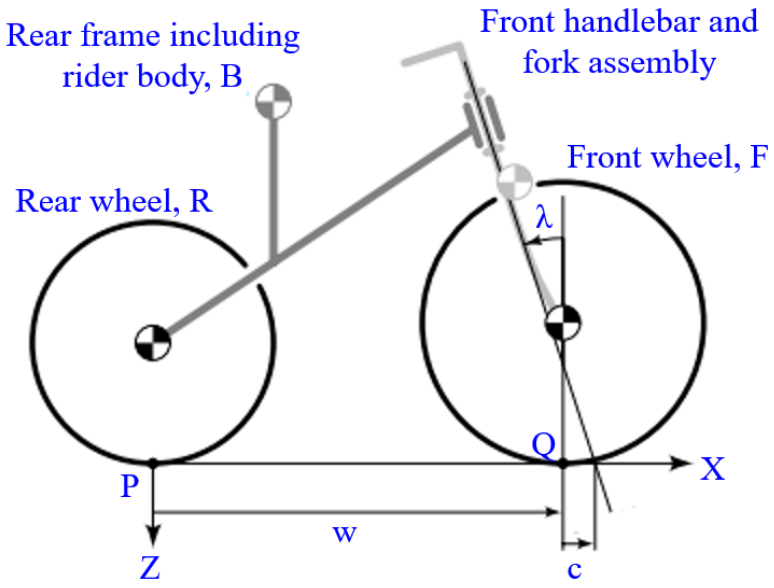

Figure 3-1. Benchmark bicycle model (Meijaard et al. 2007)

Eq. 3-2 is used to calculate the eigenvalues with an assumed solution of an exponential time-varying quantity q ($q = q_o e^{(\lambda t)}$). Eq. 3-2 yields a fourth order equation that has four distinct eigenmodes. Among them, two modes (capsize and weave mode) are important for the stability of a bicycle. The capsize mode corresponds to a real eigenvalue and eigenvector dominated by the lean. In weave mode, the bicycle steers sinuously about the headed direction with a slight phase lag relative to leaning. The castering mode is represented by the third eigenvalue that is large, real, and negative. This mode is dominated by the steer in which the front ground contact follows a tractrix-like pursuit trajectory.

The eigenvalues are functions of the bicycle velocity. The eigenvalues are plotted against velocity as shown in Figure 3-2. When the velocity is less than 4.292 m/s, the bicycle is unstable. At the weave speed (4.292 m/s), the eigenvalues crossed the imaginary axis in a Hopf bifurcation (Strogatz 1994) and become stable. When the velocity is greater than 6.0 m/s, the capsize eigenvalue crosses the origin in a pitchfork bifurcation, making the bicycle mildly unstable (Basu-Mandal et al. 2007). Within the velocity range of 4.292 ~ 6.024 m/s, the uncontrolled bicycle shows asymptotically stable behavior for all eigenvalues having negative parts. The velocity range 4.292 ~ 6.024 m/s defines the self-stable velocity region.

Table 3-1. Benchmark Bicycle Model Parameters (Meijaard et al. 2007)

Parameter	Symbol	Benchmark value
Wheel base (m)	w	1.02
Trail (m)	c	0.08
Steer axis tilt (rad)	λ	π/10
Gravitational acceleration (m/s^2)	g	9.81
Velocity (m/s)	v	Various
Rear wheel, R		
Radius (m)	r_R	0.3
Mass (kg)	m_R	2
Mass moments of inertia (kg m^2)	(I_{Rxx}, I_{Ryy})	(0.0603, 0.12)
Rear body and frame assembly, B		
Position of center of mass (m)	(x_B, z_B)	(0.3, - 0.9)
Mass (kg)	m_B	85
Mass moment of inertia (kg m^2)	$\begin{bmatrix} I_{Bxx} & 0 & I_{Bxz} \\ 0 & I_{Byy} & 0 \\ I_{Bxz} & 0 & I_{Bzz} \end{bmatrix}$	$\begin{bmatrix} 9.2 & 0 & 0 \\ 0 & 11 & 0 \\ 2.4 & 0 & 2.8 \end{bmatrix}$
Front handlebar and fork assembly, H		
Position of center of mass (m)	(x_H, z_H)	(0.90, - 0.7)
Mass (kg)	M_H	4
Mass moment of inertia (kg m^2)	$\begin{bmatrix} I_{Hxx} & 0 & I_{Hxz} \\ 0 & I_{Hyy} & 0 \\ I_{Hxz} & 0 & I_{Hzz} \end{bmatrix}$	$\begin{bmatrix} 0.05892 & 0 & 0 \\ 0 & 0.06 & 0 \\ -0.00756 & 0 & 0.00708 \end{bmatrix}$
Front wheel, F		
Radius (m)	r_F	0.35
Mass (kg)	m_F	3
Mass moments of inertia (kg m^2)	(I_{Fxx}, I_{Fyy})	(0.1405, 0.28)

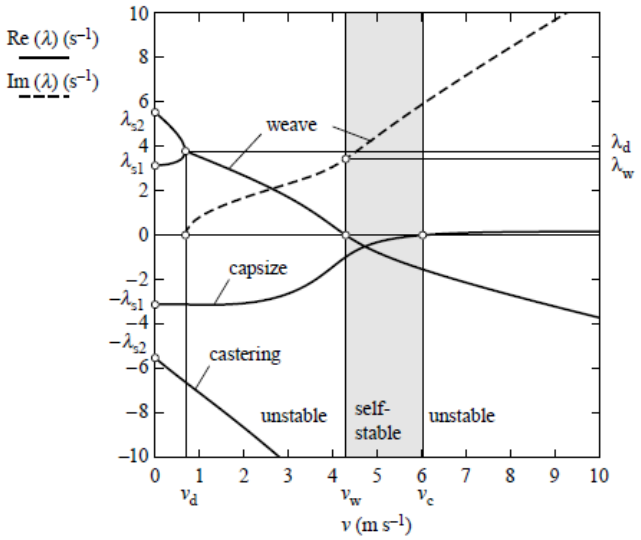

Figure 3-2. Eigenvalue vs. velocity diagram of the benchmark model (Meijaard et al. 2007)

3.3 SIMULATION MODEL IN ADAMS

A simulation model, as shown in Figure 3-3, is developed in ADAMS by replicating the Whipple benchmark bicycle model. At first, the bicycle model is simulated over an infinitely long flat road. Later, the road geometry is changed to replicate the other desired configurations. The width and aspect ratio of the tires are 52.5 mm and 0.12, respectively. The tires have properties of the ADAMS built-in tire model PAC89. Figure 3-4 shows the coordinate system used for modeling and the coordinates of the specific points of the geometry. The dimensions of the front handlebar, fork assembly, and rear frame (including the rider's body position) of the Whipple benchmark model are not provided in literature. In order to complete the model, necessary dimensions are estimated and provided in Table 3-2. As a result, there is a slight difference in center of gravity of the front handlebar and fork assembly compared to the original model presented in literature. Further, an equal value of X- and Y-axes components of mass moment of inertia of the wheels is used to define symmetric wheels. In Table 3-2, the values that are different from the original Whipple model are highlighted using underlined *italic* text. The values presented in Table 3-2 are used to calculate the eigenvalues and the corresponding velocities. A MATLAB code is developed to plot the eigenvalue vs. velocity diagram using equations presented in Appendix B. The MATLAB code is presented in Appendix C. Figure 3-5 shows the eigenvalue vs. velocity plot. The self-stable velocity range is 5.4995 ~ 8.5345 m/s (12.30 ~ 19.09 mph).

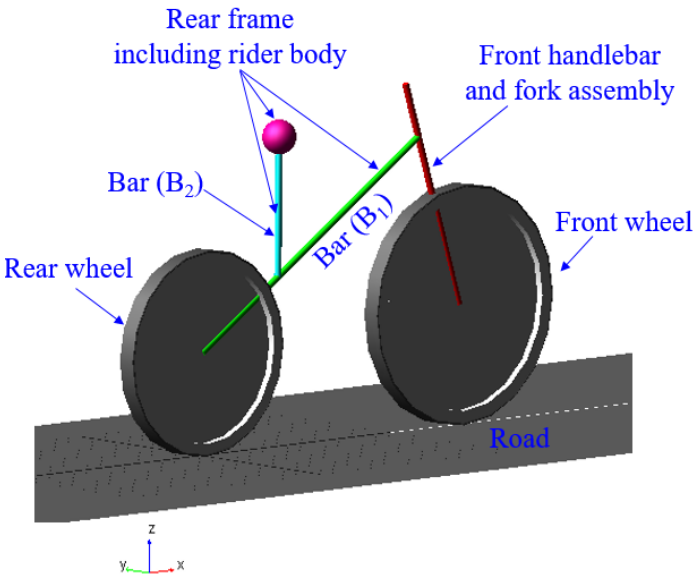

Figure 3-3. ADAMS bicycle model

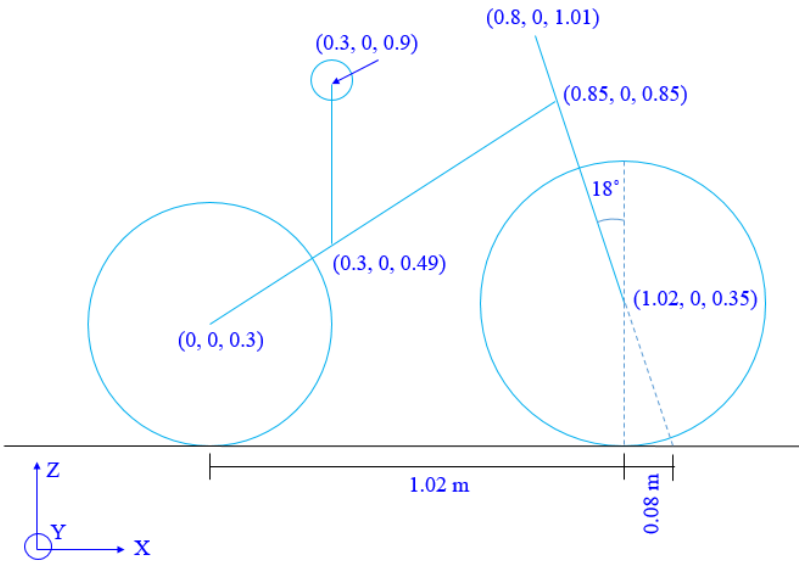

Figure 3-4. ADAMS bicycle model with coordinates

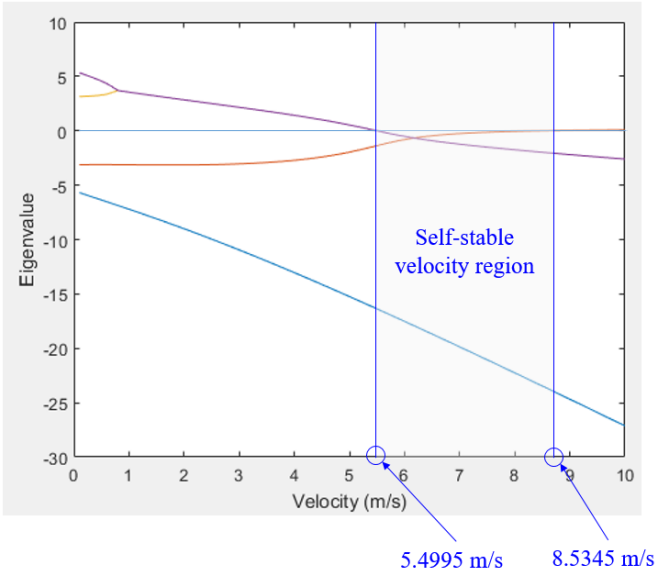

Figure 3-5. Eigenvalue vs. velocity diagram of the ADAMS bicycle model

Table 3-2. Parameters of the ADAMS Bicycle Model

Parameter	Symbol	Benchmark value
Wheel base (m)	w	1.02
Trail (m)	c	0.08
Steer axis tilt (rad)	λ	$\pi/10$
Gravitational acceleration (m/s^2)	g	9.81
Velocity (m/s)	v	Various
Rear wheel, R		
Radius (m)	r_R	0.3
Mass (kg)	m_R	2
Mass moments of inertia (kg m^2)	(I_{Rxx}, I_{Ryy})	(0.0603, *0.0603*)
Rear body and frame assembly, B		
Position of center of mass (m)	(x_B, z_B)	(0.3, 0.9)
Mass (kg)	m_B	85
Mass moment of inertia (kg m^2)	$\begin{bmatrix} I_{Bxx} & 0 & I_{Bxz} \\ 0 & I_{Byy} & 0 \\ I_{Bxz} & 0 & I_{Bzz} \end{bmatrix}$	$\begin{bmatrix} 9.2 & 0 & 0 \\ 0 & 11 & 0 \\ 2.4 & 0 & 2.8 \end{bmatrix}$
Front handlebar and fork assembly, H		
Position of center of mass (m)	(x_H, z_H)	(*0.91, 0.68*)
Mass (kg)	M_H	4
Mass moment of inertia (kg m^2)	$\begin{bmatrix} I_{Hxx} & 0 & I_{Hxz} \\ 0 & I_{Hyy} & 0 \\ I_{Hxz} & 0 & I_{Hzz} \end{bmatrix}$	$\begin{bmatrix} 0.05892 & 0 & 0 \\ 0 & 0.06 & 0 \\ -0.00756 & 0 & 0.00708 \end{bmatrix}$
Front wheel, F		
Radius (m)	r_F	0.35
Mass (kg)	m_F	3
Mass moments of inertia (kg m^2)	(I_{Fxx}, I_{Fyy})	(0.1405, *0.1405*)

The following steps are used to develop the simulation model in ADAMS. The component labels shown in Figure 3-3 and the coordinates shown in Figure 3-4 are constantly referenced during the following steps.

i. The unit system of ADAMS is set to an MKS unit system so that the unit of length, mass, force, time, and angle are in meters, kilograms, Newtons, seconds, and degrees, respectively.

ii. The gravity (9.81 m/s^2) is set along the negative Z axis.

iii. A tire having a radius of 0.3 m is added as the rear tire. The CG of the tire is at (0, 0, 0.3). Since a single tire over a road is unstable during simulation, another tire with the same properties is added at the same position with a local axis opposite to the previously added tire to have a stable tire model. These two rear tires are connected

using a fixed joint. The total mass of the tires is 2 kg. The mass moment of inertias ($I_{Fxx} = I_{Fyy} = I_{Rzz}$) is equal to 0.0603 kg m^2.

iv. Following the same procedure, a front tire of 0.35 m radius is developed and added to the model. The CG of the tires is at (1.02, 0, 0.35). The total mass of the tire is 3 kg. The mass moment of inertias ($I_{Fxx} = I_{Fyy} = I_{Rzz}$) is equal to 0.1405 kg m^2.

v. The contact points between the road and the rear and front wheels are defined. The distance between these two points is 1.02 m, or the distance of the wheel base (w).

vi. The front handlebar is added to the model as a solid cylindrical bar between points (1.02, 0, 0.35) and (0.8, 0, 1.01) so that the steer axis tilt is 18º and trail is 0.08 m. The diameter of the solid cylindrical bar is 20 mm. The CG of the handlebar is (0.91, 0, 0.68). The mass of the handlebar is 4 kg. The mass moment of inertias is I_{Hxx} = 0.05892 kg m^2, I_{Hyy} = 0.06 kg m^2, I_{Hzz} = 0.00708 kg m^2, and I_{Hxz} = – 0.00756 kg m^2.

vii. A 20 mm diameter solid cylindrical bar (B_1) is used to connect the front handlebar at (0, 0, 0.3) and the center of the rear wheel at (0.85, 0, 0.85). The total mass and mass moment of inertia is acting on the CG of four parts of the benchmark bicycle model. Therefore, the mass and mass moment of inertia of this connecter are not included in the model (i.e., a zero value is assigned to both of these parameters).

viii. A solid ellipsoid of 85 kg is added at (0.3, 0, 0.9) to represent the rider. The moments of inertia are I_{Bxx} = 9.2 kg m^2, I_{Byy} = 11 kg m^2, I_{Bzz} = 2.8 kg m^2, and I_{Bxz} = 2.4 kg m^2.

ix. Another 20 mm diameter solid cylindrical bar (B_2) is used to connect the bar B_1 at (0.85, 0, 0.85) and the center of the ellipsoid at (0, 0, 0.3). The total mass and mass moment of inertia are acting on the CG of four parts of the benchmark bicycle model. Therefore, the mass and mass moment of inertia of this connecter are not included in the model (i.e., a zero value is assigned to both of these parameters).

x. A fixed joint is assigned at (0.3, 0, 0.9) to establish the connection between the ellipsoid and bar B_2.

xi. A fixed joint is assigned at (0.3, 0, 0.49) to establish the connection between bar B_1 and B_2.

xii. A revolute joint is assigned at (1.02, 0, 0.35) to define the connection between the front wheel and the handlebar assembly.

xiii. A revolute joint is assigned at (0, 0, 0.3) to define the connection between the rear wheel and the bar B_1.

xiv. A fixed joint is assigned at (0.85, 0, 0.85) to define the connection between the handlebar assembly and the bar B_1. Figure 3-6 shows all the assigned joints in the model.

xv. Two markers are added to the rear and front wheels at (0, 0, 0) and (1.02, 0, 0). These markers are used to assign the contact properties.

xvi. A Spline is constructed to represent the road geometry.

xvii. In order to define the bicycle travel path along the predefined road (the Spline defined in the previous step), planar joints and point-to-curve contacts are assigned. For the simulation described in this chapter, two simulation models are used: (i) one model with front and rear wheels constrained to the curve and (ii) the other model with only the front wheel constrained to the curve. The interaction schemes are presented in Table 3-3. Figure 3-7 shows the planar joint(s) and the point-to-curve contact(s) for each scheme.

Table 3-3. Planar Joint and Point-to-Curve Contact Schemes

Scheme	Geometry	Planar joint/contact location (m)
1	Front wheel/Curve	(1.02, 0 , 0)
	Rear wheel/Curve	(0, 0, 0)
2	Front wheel/Curve	(1.02, 0 , 0)

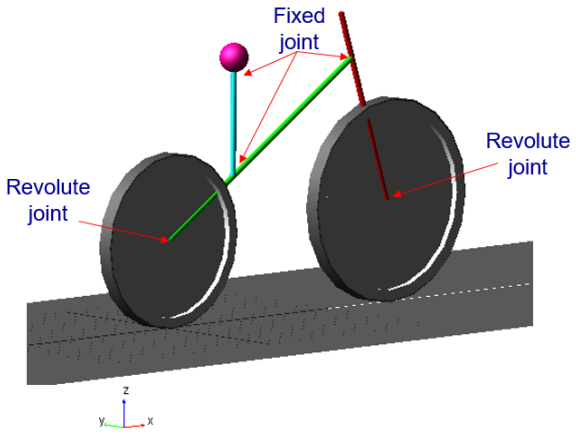

Figure 3-6. Joint definitions

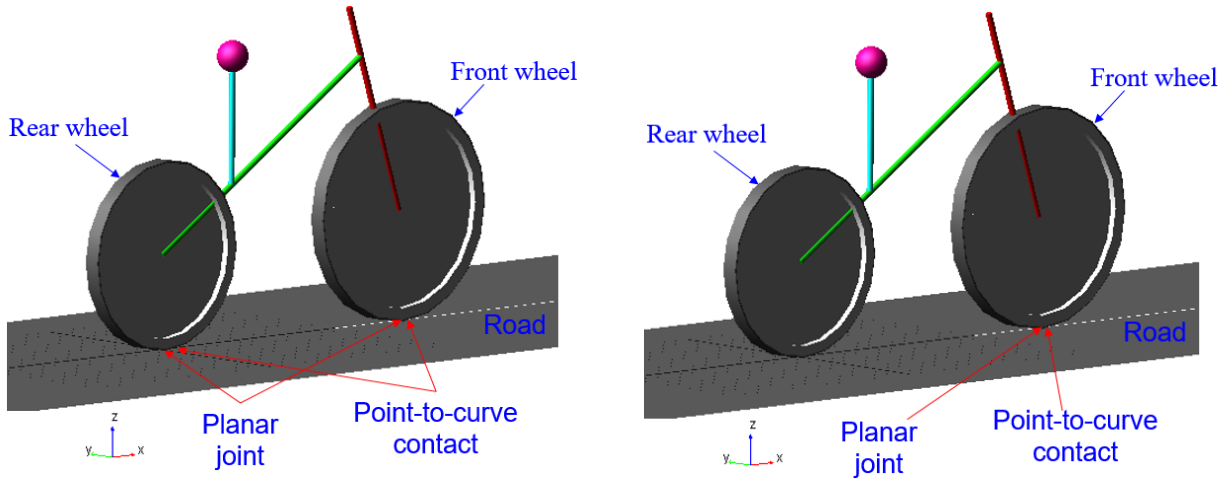

Scheme 1 Scheme 2

Figure 3-7. Planar joint(s) and point-to-curve contact(s) between wheel and curve

3.4 MODEL VALIDATION

The ADAMS bicycle model is validated using force equilibrium, centripetal acceleration, and the data collected using an instrumented probe bicycle (IPB).

3.4.1 Force Equilibrium

The total weight of the bicycle is transferred to the ground through two contact points as shown in Figure 3-8. The CG of the bicycle is at (0.343, 0, 0.860) m from the rear wheel contact point. The reaction forces calculated by considering equilibrium are presented in Figure 3-8b. The theoretical vertical (Z-axis) reaction forces at the front and rear wheel contact points are 310.09 and 612.05 N, respectively. The reactions calculated using ADAMS software are 309.98 and 612.34 N, respectively. Hence, a very good correlation between theoretical and simulation results is observed.

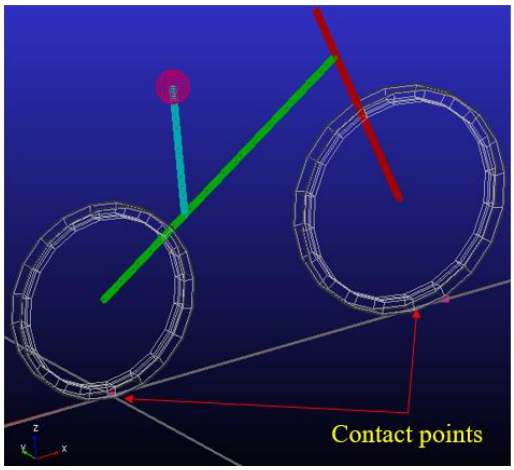

a) Contact points between wheels and the road surface

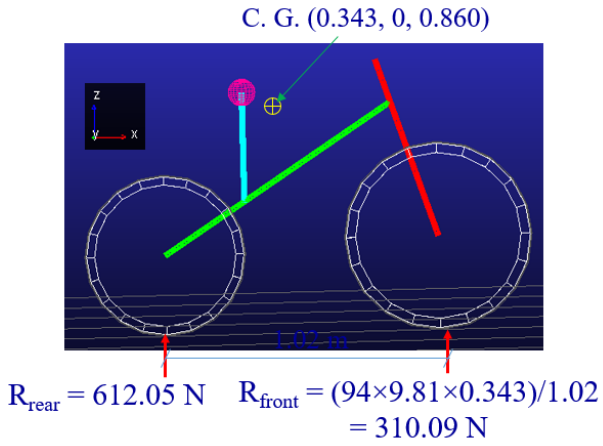

b) Vertical reactions at the contact points

Figure 3-8. Bicycle contact points and the vertical reactions

3.4.2 Centripetal Acceleration

A road segment within the Parkview campus of Western Michigan University (WMU) is selected and replicated in the software as shown in Figure 3-9 and Figure 3-10. This road is nearly flat and composed of a conventional bike lane and 3 curves. Figure 3-9b shows the geometry and the radii of the curves.

The Google map image of the bikeway route is processed in AutoCAD. Lines and curves are fitted onto the route using available tools in AutoCAD to accurately replicate the route. Several points are needed to create a smooth curve in ADAMS. Each of the route segments is divided in to 50 points using the DIVIDE command in AutoCAD. Using the LIST command, the coordinates are copied from AutoCAD to Microsoft Excel. The Text to Columns command is used to separate X, Y, and Z axis coordinates into columns. Coordinates of all the segments are copied to the ADAMS road input file and used for developing the road geometry.

The bicycle movement along this path was simulated at a constant velocity of 7.03 m/s. Table 3-4 shows the centripetal accelerations (theoretical and simulation results) when the bicycle travels along these three curves. For the simulation, the bicycle model with two contact points (scheme 1) was used. The results show a very good agreement.

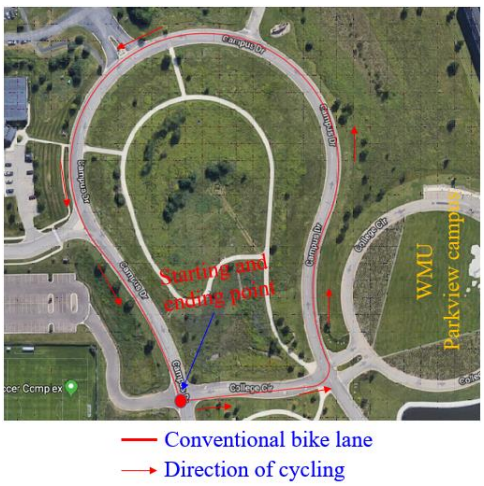

a) Google image of the road segment

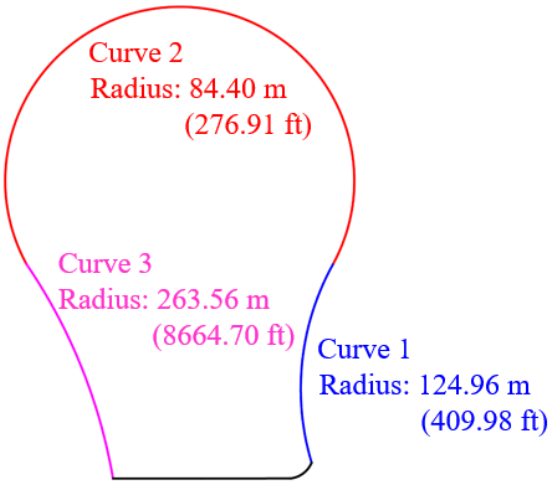

b) Radii of the curves

Figure 3-9. Road segment geometry

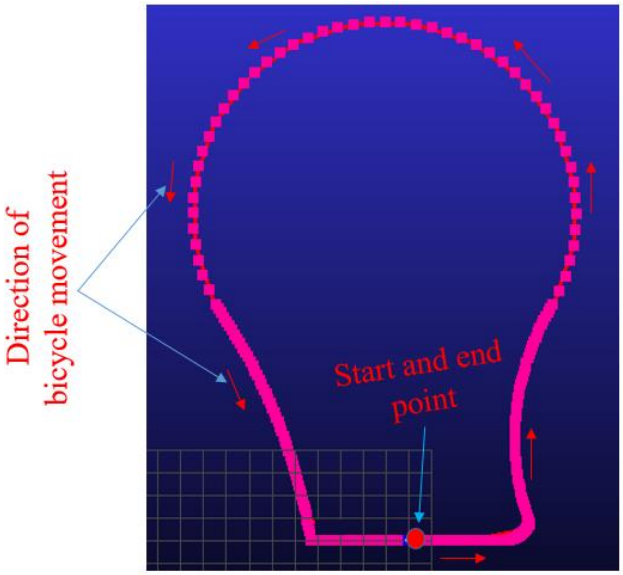

Figure 3-10. Road segment modeled in ADAMS

Table 3-4. Centripetal Acceleration

Curve no.	Centripetal acceleration (m/s^2)	
	Theoretical (V^2/R)	Simulation
1	0.39	0.44
2	0.58	0.54
3	0.19	0.19

3.4.3 Experimental Validation

The simulation model presented in Figure 3-7a (Scheme 1) is validated using experimental data collected using an instrumented probe bicycle (IPB) that is capable of measuring acceleration,

velocity, location (latitude, longitude, and altitude), lean angle, pitch angle, and yaw angle in a fixed time interval (Oh et al. 2017). The IPB and the sensor layout are shown in Figure 3-11 and Figure 3-12.

Figure 3-11. Instrumented probe bicycle (IPB) (Oh et al. 2017)

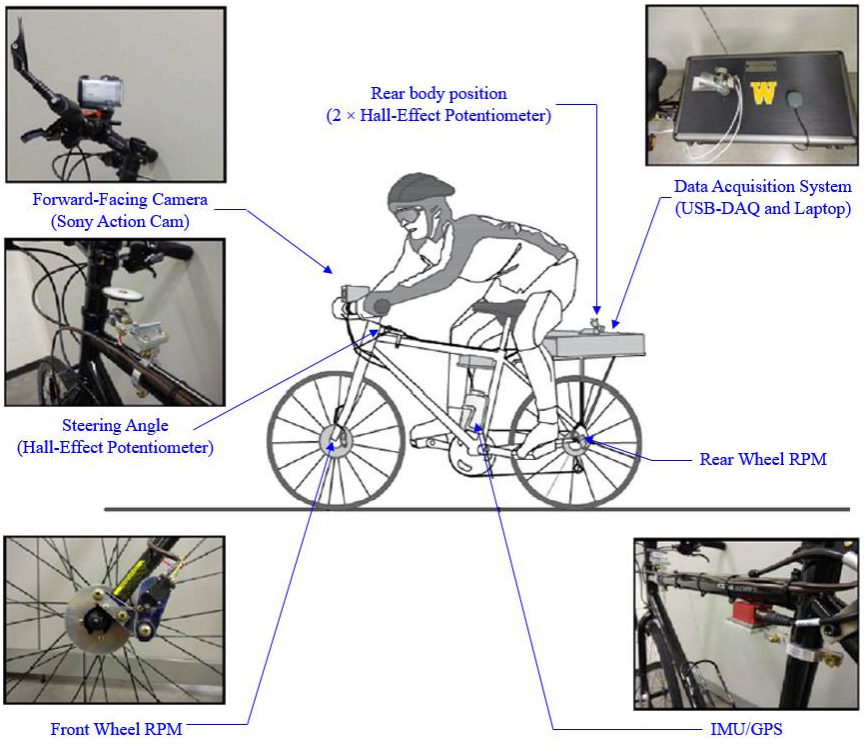

Figure 3-12. Instrumentation layout of the IPB (Oh et al. 2017)

The jerk was calculated using acceleration data. Figure 3-13a shows the jerk and velocity variation against time when the bicycle travelled along curve 2. Jerk at the entrance and exit of the curve is 4.59 m/s^3 and 1.54 m/s^3. As shown in Figure 3-13a, there is no sudden change in the velocity as the bicycle enters and exits the curve. Hence, the sudden increase in jerk at the

entrance to curve 2 can be attributed to the change in radius and/or the direction of the curve. As shown in Figure 3-13b, there is a sudden change in the lean angle. This is primarily due to the change in the direction of curves as well as the radii that required leaning the bicycle in different directions to maintain stability. Hence, a sharp increase of the jerk is observed at the entrance to the curve. At the exit of the curve, there is no sudden change in the velocity or the lean angle since there is a smoother transition between curve 2 and curve 3. Hence, a much smaller jerk is observed. As the bicycle travelled along curve 2, the cyclist leaned the bicycle side-to-side (Figure 3-13b). These changes are reflected as the spikes of jerk within the curve. The road surface was not smooth and included regular cracks and crack treatments (Figure 3-14). These irregularities could have contributed to the small changes in the jerk when the bicycle was leaned as it travelled along the curve.

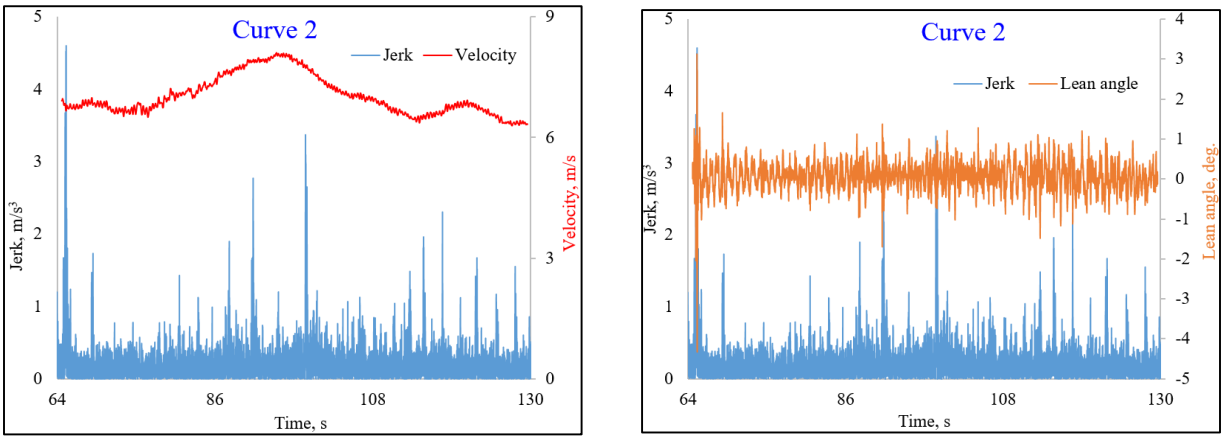

a) Jerk and velocity variation against time b) Jerk and lean angle variation against time

Figure 3-13. Jerk, velocity, and lean angle variation against time - curve 2

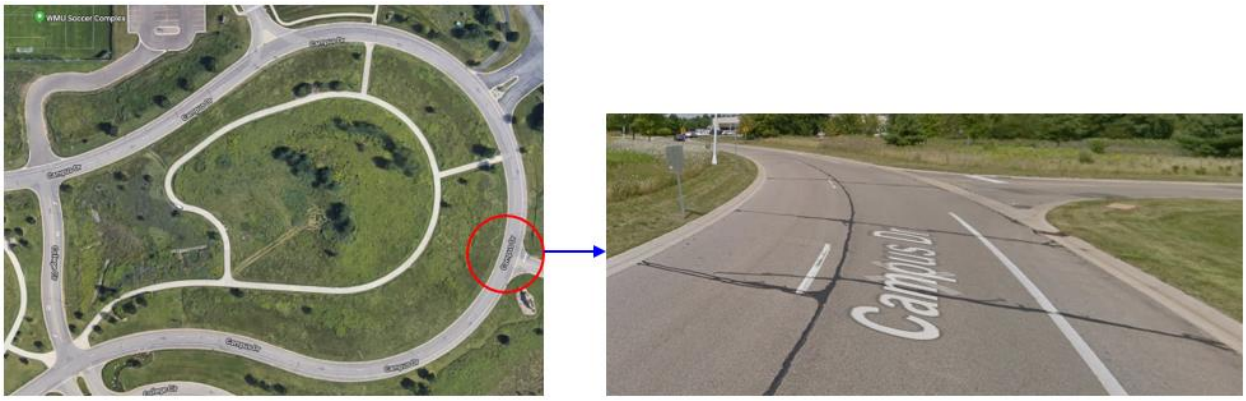

Figure 3-14. Road surface condition

Bicycle movement along the defined path was simulated at a constant speed of 7.03 m/s (15.73 mph). Jerk is calculated using simulation results for curve 2. Figure 3-15a and Figure 3-15b show the variation of jerk against time obtained from experimental data and simulation results, respectively. The jerk calculated using experimental data and simulation results at the entrance to curve 2 is 4.59 m/s^3 and 4.77 m/s^3, respectively. Also, the jerk calculated using experimental data and simulation results at the exit of curve 2 is 1.54 m/s^3 and 1.40 m/s^3, respectively. The results show a very good agreement.

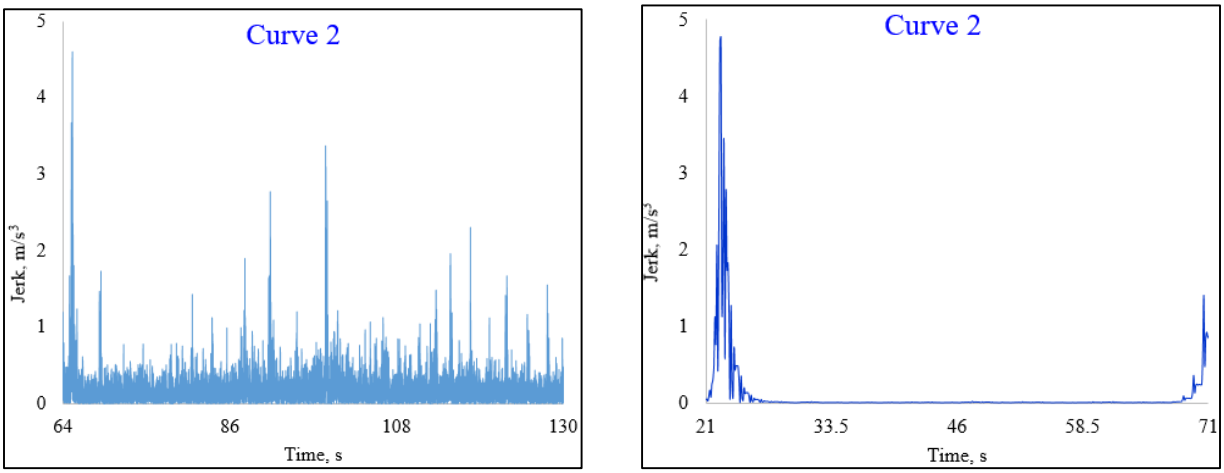

a) Jerk calculated using IPB data b) Jerk calculated using simulation results

Figure 3-15. Variation of jerk against time when travelling along curve 2

3.5 SUMMARY

The mathematical models to describe dynamic behavior and stability of a bicycle have been studied for more than 140 years. Meijaard et al. (2007) presents the Whipple model, the most widely used benchmark bicycle model, and its design parameters. This model is replicated as a simulation model in ADAMS and verified theoretically by considering force equilibrium and centripetal acceleration. Later, the model was validated using experimental data collected using an instrumented probe bicycle (IPB). The theoretical and experimental validations proved capabilities and reliability of the model to be used for further analysis.

4 EVALUATION OF BIKEWAY DESIGN PARAMETERS

4.1 OVERVIEW

Chapter 3 presented the simulation model development and validation. The experimental route used for model validation included only 3 curves. This chapter presents the use of a more complicated route for simulation. The evaluation results presented in this chapter include the impact of curvature, speed, and transition curves on stability and comfort.

4.2 ROUTE FOR SIMULATION

A route located near the Western Michigan University (main campus) is selected (Figure 4-1). Even though this route has a grade, the simulation is performed considering it as a flat road. Figure 4-1a shows the direction of cycling. However, in order to match with the positive axes of the coordinate system in ADAMS, the route is mirrored as shown in Figure 4-1b. Total length of the route is 1.35 km. Figure 4-2 shows the route with actual dimensions of all the road segments. The route has two classes of bikeway: i) shared roadway and ii) conventional bike lane. Figure 4-3a shows the route with different classes of bikeway. As shown in Figure 4-3b, this route is composed of several curves with different degrees of curvature.

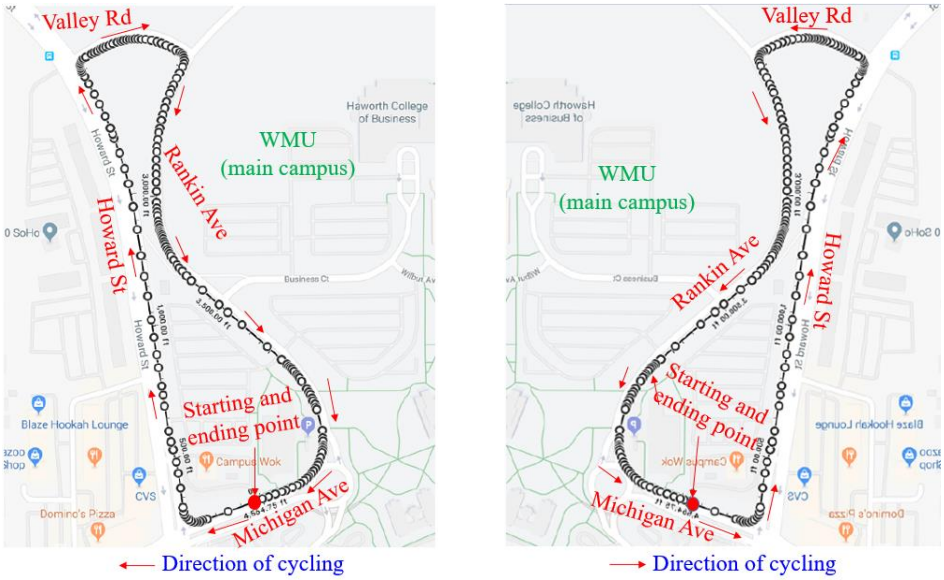

a) Geometry and orientation of the route

b) Mirrored route to match positive axes of the coordinate system used in ADAMS

Figure 4-1. Selected bikeway geometry and orientation (Location: 42.282115, -85.620601)

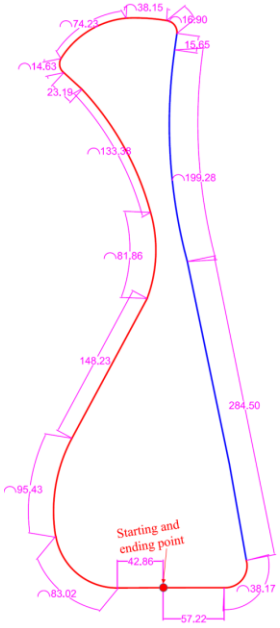

Figure 4-2. Road segment length (in meters)

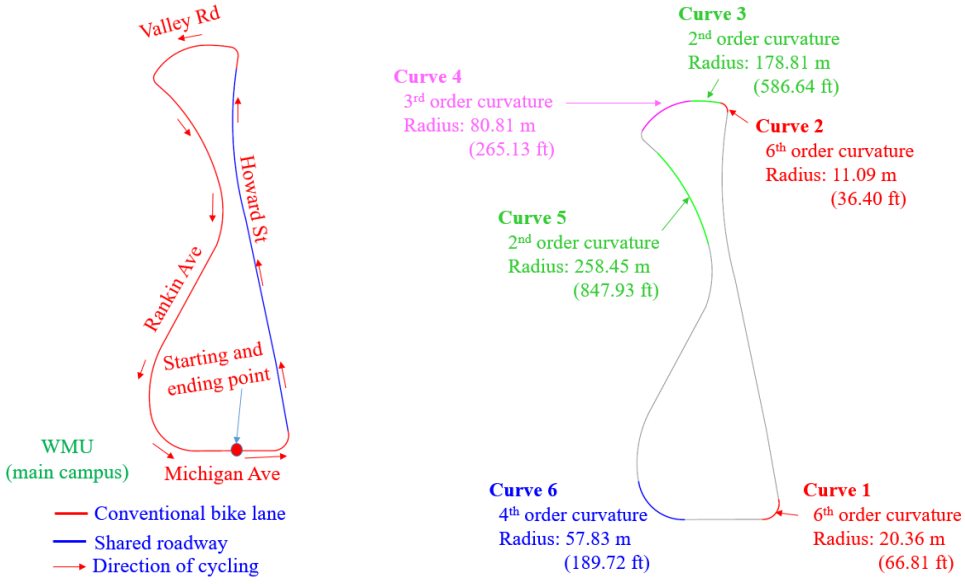

a) Bikeway route b) Curvature and radii information

Figure 4-3. Bikeway route and curvature and radii information

Following a similar procedure, as described in chapter 3, the route is modeled in ADAMS as shown in Figure 4-4.

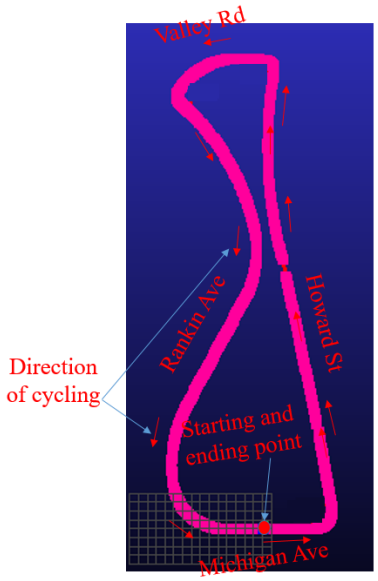

Figure 4-4. The bikeway model in ADAMS

4.3 SIMULATION VELOCITY

The self-stable velocity range of the model is 5.4995 ~ 8.5345 m/s (12.30 ~ 19.09 mph). Five different velocities are selected for simulation and shown in Table 4-1. All these velocities are in the self-stable velocity range. Since the benchmark model parameters are in SI units, all the simulation results are presented using that unit system. Where needed, Imperial Units are used.

Table 4-1. Bicycle Velocity Used in Simulation

Velocity	
mph	**m/s**
12.5	5.59
14.0	6.26
15.5	6.93
17.0	7.60
18.5	8.27

4.4 CONTACT FORCES AND CENTRIPETAL ACCELERATION

Centripetal acceleration, thus the centrifugal force, is developed when a bicycle is travelling along a horizontal curve. To maintain the bicycle position along a defined path, planar joints and point-to-curve contacts are assigned. As shown in Figure 3-7, two schemes are defined: (i) scheme 1 – where the contacts are defined at the front and rear wheels, and (ii) scheme 2 – where contact is defined only at the front wheel. The planar joint and point-to-curve contact guide the bicycle along the curve. As a result, contact forces are developed at the contact points. The resultant of these contact forces is equal and opposite to the centrifugal force when the bicycle is

in equilibrium. Figure 4-5 shows the forces acting on a point-mass system when it travels along a curve. Figure 4-6a and Figure 4-6b show the contact forces at the front and rear wheels when the bicycle is travelling at a speed of 6.93 m/s, and forces are higher within the curve. Contact forces at the rear wheel are higher than the front wheel since the vertical load at the rear wheel is greater.

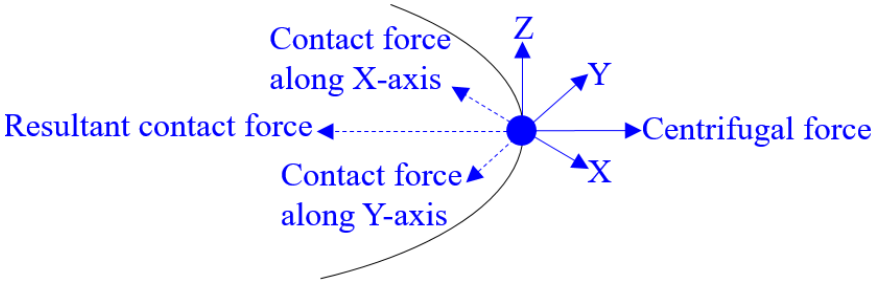

Figure 4-5. Contact forces and centrifugal forces in a curve

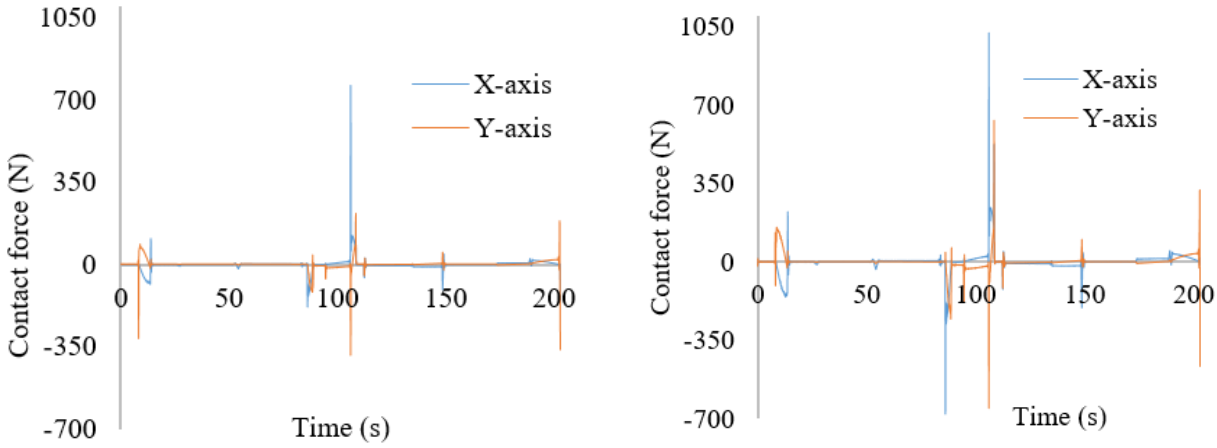

a) Front wheel contact force b) Rear wheel contact force

Figure 4-6. Front and rear wheel contact forces as the bicycle travels along the curve

Centripetal acceleration is calculated for each time increment. ADAMS average centripetal acceleration is calculated within a horizontal curve using centripetal acceleration of each time increment. Table 4-2 shows the ADAMS average and theoretical centripetal acceleration for different velocities and degrees of curvature. Average centripetal acceleration within a curve is close to the theoretical value for a given simulating velocity and degree of curvature. The centripetal acceleration increases with the increase of velocity and degree of curvature.

Table 4-2. Centripetal Acceleration for Various Simulation Velocities and Degrees of Curvature

Curve no. (Degree of curvature)	Centripetal acceleration (m/s^2)									
	5.89 m/s (12.5 mph)		6.26 m/s (14.0 mph)		6.93 m/s (15.5 mph)		7.60 m/s (17.0 mph)		8.27 m/s (18.5 mph)	
	A[1]	T[2]	A	T	A	T	A	T	A	T
2 (6)	2.75	2.81	3.18	3.29	3.99	3.95	4.62	5.05	6.06	6.07
3 (2)	0.19	0.17	0.19	0.19	0.26	0.23	0.31	0.31	0.38	0.38
4 (3)	0.38	0.38	0.44	0.42	0.51	0.51	0.66	0.69	0.79	.83
6 (4)	0.47	0.46	0.58	0.58	0.61	0.61	0.87	0.94	1.11	1.13

1. ADAMS average centripetal acceleration (m/s^2)
2. Theoretical centripetal acceleration (m/s^2)

4.5 SLIP ANGLE

The bicycle is simulated with scheme 1 for different velocities that are listed in Table 4-1. The slip angles of the rear wheel for different degrees of curvature are recorded and plotted against the simulation velocity. Figure 4-7 shows the graph for different velocities and degrees of curvature. Slip angle increases with the increase of velocity and degree of curvature. The magnitude of the slip angle also depends on the availability of transition curves at the entrance and exit of a horizontal curve. Slip angle is the greatest at the 4th order curve as the bicycle leaves Curve 6 and enters a straight line. On the other hand, the slip angle is lower when the bicycle travels along the 6th order curve (Curve 2) and enters into the 2nd order curve (Curve 3) due to a little smoother transition at the exit than that of the 4th order curve.

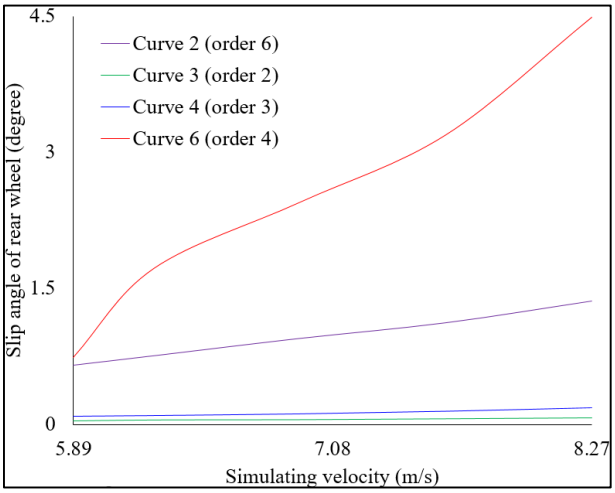

Figure 4-7. Variation of slip angle against the simulation velocity

4.6 VARIATION OF CENTRIPETAL ACCELERATION AND JERK

Simulation results show a variation of centripetal acceleration when the bicycle is travelling along the curve while the theoretical value is a constant. The simulation was performed at a velocity of 6.93 m/s. The variation of centripetal acceleration, average value of the simulation results, and the theoretical value are presented in Figure 4-8 to Figure 4-10 for all 6 curves. Figure 4-11 shows the variation of centripetal acceleration at 5.59 m/s and 8.27 m/s velocities when the bicycle is travelling along the 6th order curve. The standard deviation of centripetal acceleration at 5.59 m/s and 8.27 m/s velocities is 0.04 m/s^2 and 0.12 m/s^2, respectively. The variation of centripetal acceleration increases with the increase of velocity and degree of curvature. Wheels of the bicycle show tractrix-like pursuit trajectory like grocery cart due to change in centripetal acceleration even though the bicycle is in a self-stable velocity region. The cyclist feels discomfort and tends to lose control and stability when subjected to greater changes of centripetal acceleration.

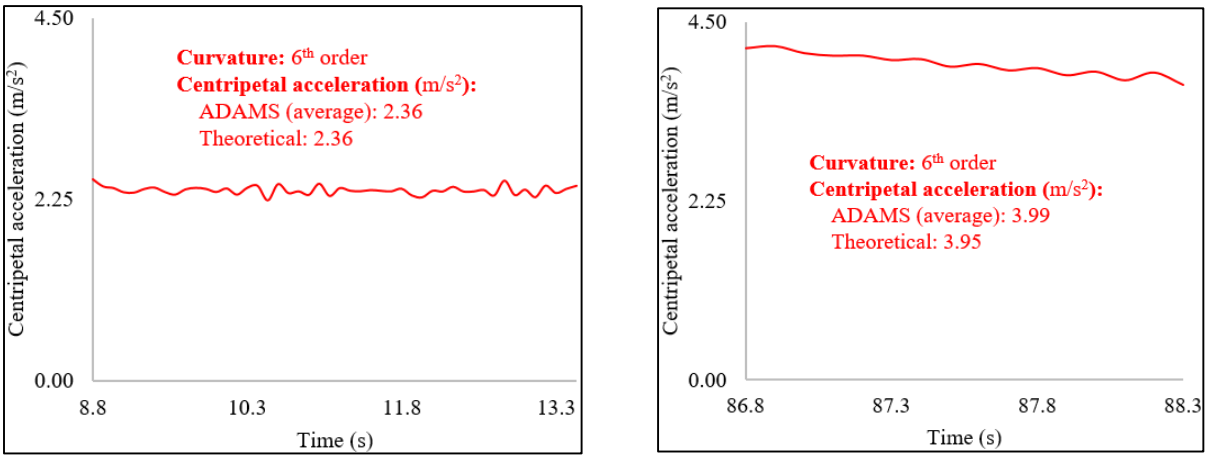

a) Curve 1 b) Curve 2

Figure 4-8. ADAMS and theoretical centripetal acceleration for curves 1 and 2 at 6.93 m/s simulating velocity

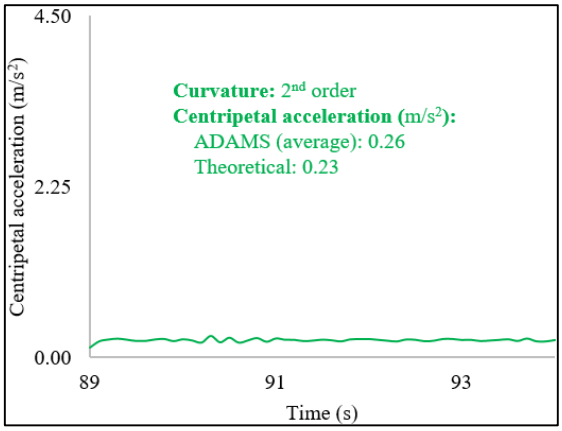

c) Curve 3

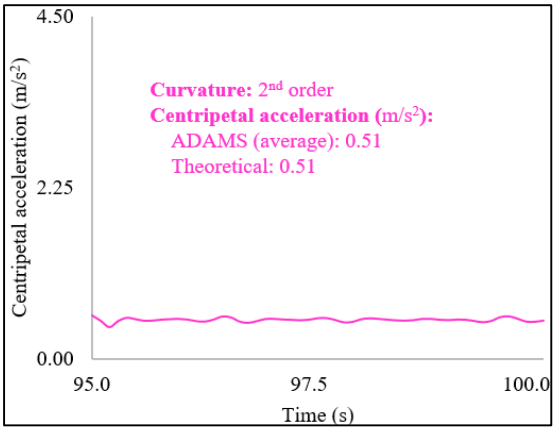

d) Curve 4

Figure 4-9. ADAMS and theoretical centripetal acceleration for curves 3 and 4 at 6.93 m/s simulating velocity

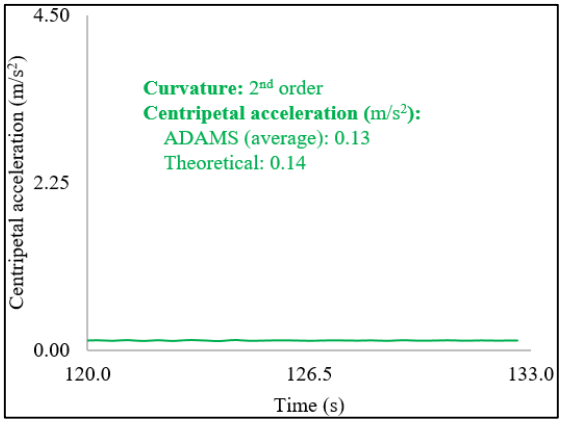

e) Curve 5

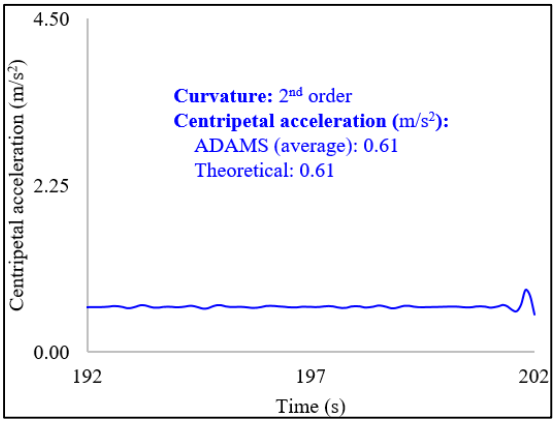

f) Curve 6

Figure 4-10. ADAMS and theoretical centripetal acceleration for curves 5 and 6 at 6.93 m/s simulating velocity

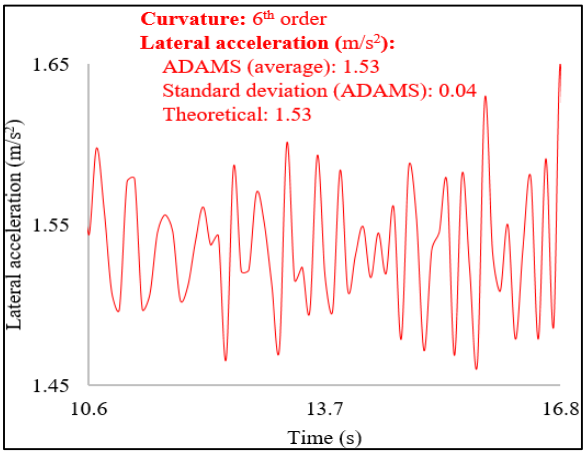

a) Simulating velocity is 5.59 m/s

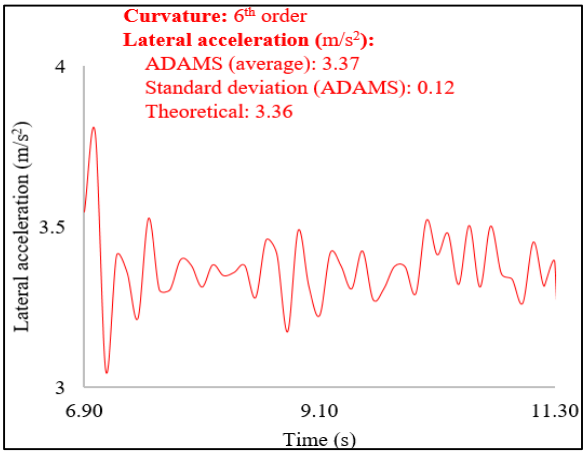

b) Simulating velocity is 8.27 m/s

Figure 4-11. Variation of centripetal acceleration when travelling along the 6th order curve at different velocities

The centripetal acceleration is changing within a horizontal curve. The rate of change for centripetal acceleration is defined as the jerk. Jerk is changing with respect to time as the centripetal acceleration is changing with respect to time. Jerk is higher at the entrance and exit of a horizontal in the absence of a proper transition curve. Figure 4-12 shows the variation of jerk for curves 1 and 2 at 6.93 m/s velocity. At curve 1, the bicycle enters from a straight line segment to the 6th order curve and leaves to another straight line segment. The transitions between the straight-line segments and the 6th order curve are not smooth. This results in a jerk of 44.82 m/s^3 and 13.02 m/s^3 at the entrance and exit of the curve, respectively. The average jerk is 0.60 m/s^3 within the curve. At curve 2, the jerk at entrance is 63.17 m/s^3 as the bicycle travels from a straight line segment to the 6th order curve. When the bicycle leaves the 6th order curve and enters the 2nd order curve, the jerk is 13.15 m/s^3. The average jerk within the 6th order curve is 0.63 m/s^3.

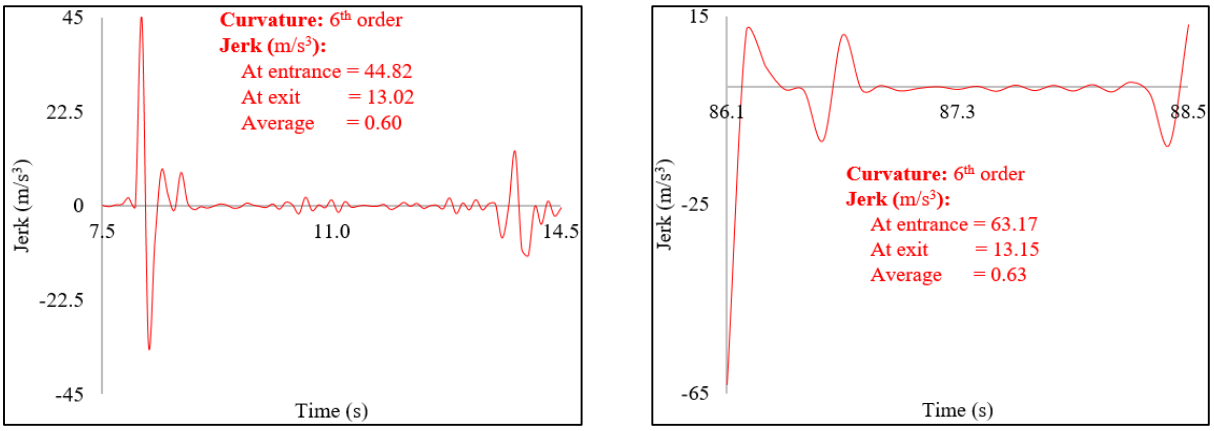

a) Variation of jerk for curve 1

b) Variation of jerk for curve 2

Figure 4-12. Variation of jerk for curves 1 and 2 at 6.93 m/s simulating velocity

Figure 4-13 shows variation of jerk for curves 3 and 4 at 6.93 m/s simulation velocity. At curve 3, bicycle enters from a 6th order curve and leaves to a 3rd order curve. The transitions between the curves are little bit smooth. This results in a jerk of 13.15 m/s^3 and 0.17 m/s^3 at the entrance and exit of the curve, respectively. The average jerk is 0.17 m/s^3 within the curve. At curve 4, the jerk at entrance is 0.17 m/s^3 as the bicycle travels from a 2nd order curve to the 3rd order curve. When the bicycle leaves the 3rd order curve and enters a curve, the jerk is 0.14 m/s^3. The average jerk within the curve is 0.09 m/s^3.

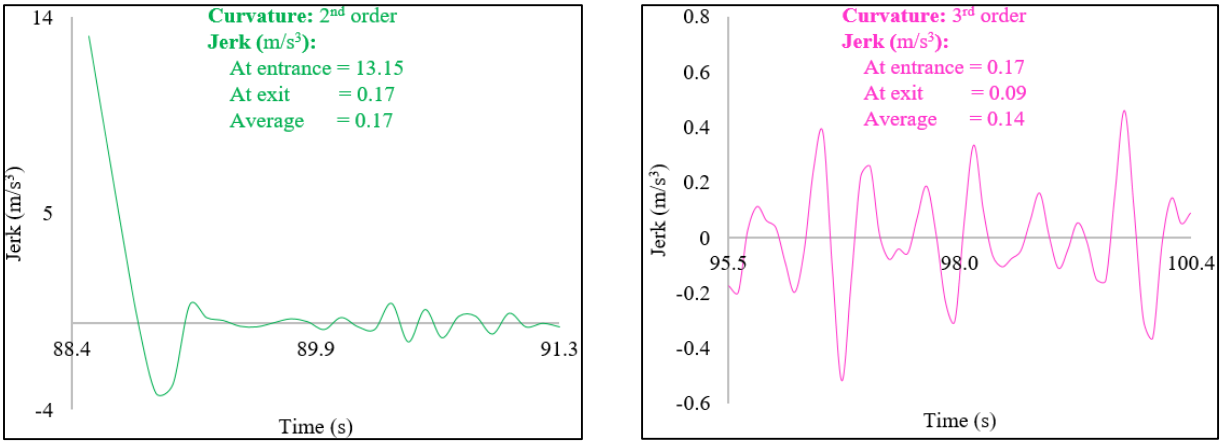

a) Variation of jerk for curve 3 b) Variation of jerk for curve 4

Figure 4-13. Variation of jerk for curves 3 and 4 at 6.93 m/s simulating velocity

Figure 4-14 shows the variation of jerk for curves 5 and 6 at 6.93 m/s simulating velocity. At curve 5, the bicycle enters from a curve and leaves to another curve. The transitions between the curves are smooth. This results in a jerk of 0.02 m/s^3 and 1.06 m/s^3 at the entrance and exit of the curve, respectively. The average jerk is 0.04 m/s^3 within the curve. At curve 6, the jerk at entrance is 0.08 m/s^3 as the bicycle travels from a 4th order curve to the 4th order curve. When the bicycle leaves the 4th order curve and enters a straight line segment, the jerk is 513.42 m/s^3. The average jerk within the curve is 0.51 m/s^3.

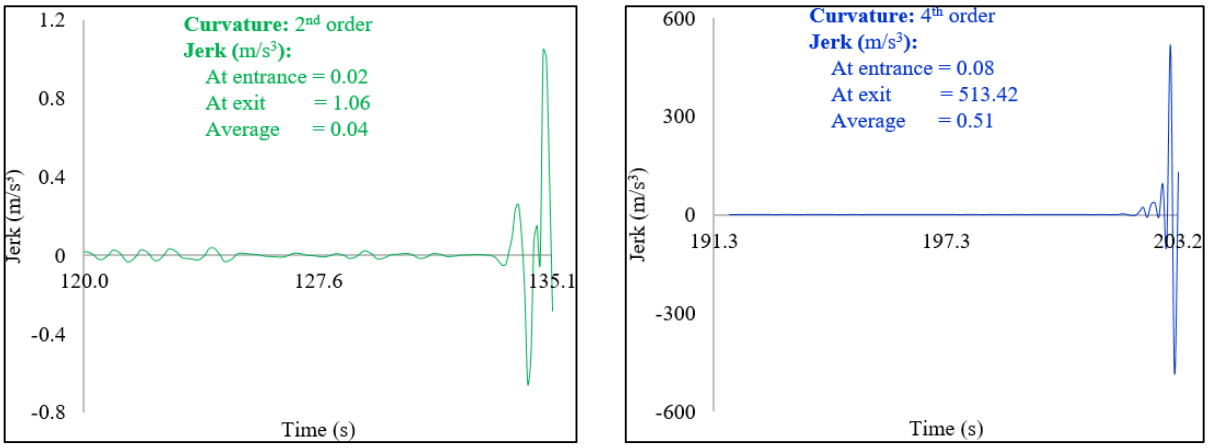

a) Variation of jerk for curve 5 b) Variation of jerk for curve 6

Figure 4-14. Variation of jerk for curves 5 and 6 at 6.93 m/s simulating velocity

Table 4-3 shows jerk at the entrance and exit of different horizontal curves located along the route. The table shows the curve number, degree of curvature, and the jerk at different velocities. Jerk increases with increase in velocity and degree of curvature. Jerk is higher in the absence of transition curves, especially when the bicycle is travelling from a straight line

segment to 6th order curve. AASHTO (2011) provides 0.3 – 0.9 m/s^3 (1 – 3 ft/s^3) as the limit of jerk for motor vehicles. According to that limit, the values observed from simulation are much greater. Since the cyclist leans as a bicycle negotiates a curve, adequacy of such limits needs to be investigated.

Table 4-3. Jerk Recorded at the Entrance and Exit of the Curves

Curve no. (Degree of curvature)	Jerk (m/s^3)									
	5.89 m/s (12.5 mph)		6.26 m/s (14.0 mph)		6.93 m/s (15.5 mph)		7.60 m/s (17.0 mph)		8.27 m/s (18.5 mph)	
	S[1]	E[2]	S	E	S	E	S	E	S	E
2 (6)	27.94	10.17	38.28	10.41	63.17	13.15	68.74	16.16	122.31	40.98
3 (2)	10.17	0.002	10.41	0.10	13.15	0.17	16.16	0.38	40.98	0.45
4 (3)	0.002	0.05	0.10	0.05	0.17	0.09	0.38	0.11	0.45	0.14
6 (4)	0.07	141.01	0.06	391.43	0.08	513.42	0.21	601.71	0.50	759.92
1. At the entrance of the curve 2. At the exit of the curve										

4.7 DESIGN OF TRANSITION CURVE USING JERK

The jerk is higher at the entrance and exit of a horizontal curve in the absence of transition curves. The cyclist feels discomfort and requires negotiating the curve with reduced speed and an appropriate lean under such conditions. Hence, transition curves are provided to increase the stability and ride comfort. The MnDOT (2007) recommendation is to provide at least a 25 ft long transition curve. It is not clear if this recommendation considers the degree of curvature of the curves. Besides, providing a 25 ft long transition curve in general might not adequately reduce jerk to a comfort level. According to Eq. 2-4 (AASHTO 2011), the length of transition curve is inversely proportional to the radius and linearly proportional to the cubic power of the velocity. Also, Eq. 2-4 shows that the jerk is linearly proportional to the cubic power of velocity, for a given transition curve length and a radius of curvature. In order to calculate the required transition curve length, using Eq. 2-4 for a given radius and a velocity range, a value for jerk is needed. Eq. 2-5 presented by IRC (2010) is available for calculating the jerk. However, Eq. 2-5 shows that the jerk is inversely proportional to the velocity, which contradicts with Eq. 2-4 and general understanding of the parameters contributing to jerk. AASHTO (2011) defines jerk limits of 0.3 – 0.9 m/s^3 (1 – 3 ft/s^3) for highways. Table 4-4 shows the average values of jerk calculated using simulation results for different curves at 6.93 m/s velocity and the length of transition curves calculated using Eq. 2-4. The average jerk of curve 1 is 0.60 m/s^3. Using this average jerk and Eq. 2-4, the length of a transition curve is calculated as shown below. The

required length of the transition curve is 90 ft. Hence, two 90 ft transition curves were provided at the beginning and end of curve 1 and the simulation results with a velocity of 6.93 m/s are shown in Figure 4-15. As shown in the figure, after providing the transition curves, jerk is reduced from 44.82 m/s^3 to 3.07 m/s^3 at the entrance and from 13.02 m/s^3 to 3.69 m/s^3 at the exit.

Sample calculation:

Velocity, V = 15.5 mph

Radius, R = 66.81 ft

Jerk, C = 0.60 m/s^3 = 1.97 ft/s^3

Length of the transition curve, $Ls = \frac{3.15V^3}{CR} = \frac{3.15\times15.5^3}{1.97\times66.81} \approx 90$ ft

Table 4-4. Average Jerk from ADAMS at 6.93 m/s (15.5 mph) Velocity and the Required Transition Curve Length Calculated Using Eq. 2-4

Curve no. (degree of curvature)	ADAMS average jerk		Length of a transition curve from Eq. 2-4 with ADAMS average jerk	
	(m/s^3)	(ft/s^3)	m	ft
1 (6)	0.60	1.97	27.43	90
2 (6)	0.63	2.07	47.55	156
3 (2)	0.34	1.12	5.49	18
4 (3)	0.14	0.46	-	-
5 (2)	0.04	0.13	-	-
6 (4)	0.51	1.67	11.28	37
The legend for curve numbers	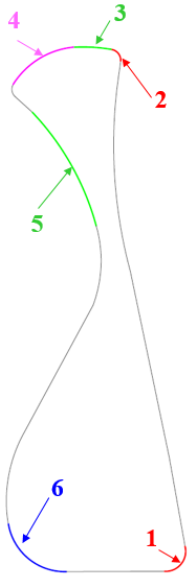			

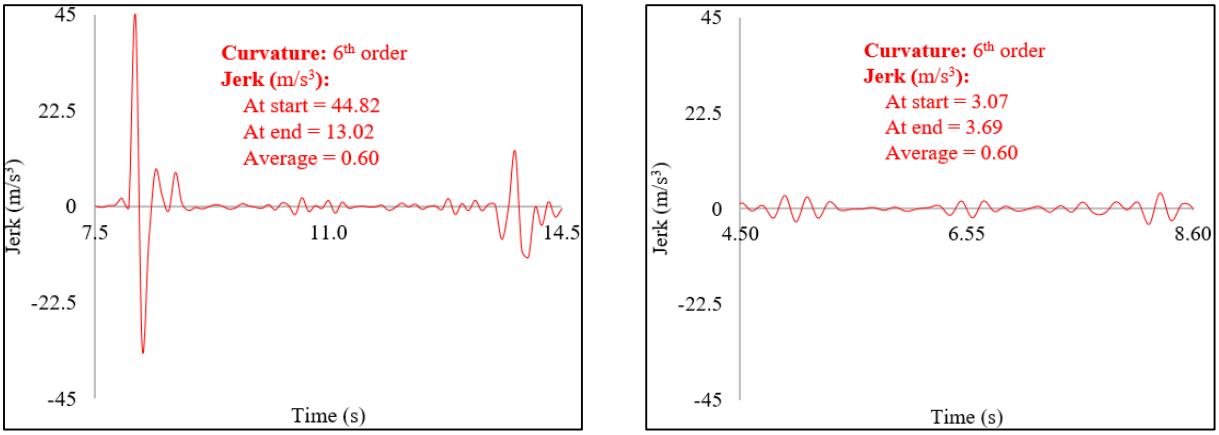

a) Before providing transition curve

b) After providing transition curve

Figure 4-15. Variation of jerk when the bicycle travels along curve 1 at a velocity of 6.93 m/s

Table 4-5 shows the average jerk calculated using simulation results at three different curves and the corresponding velocities. The curves are defined with respect to the degree of curvature. Figure 4-16 shows the variation of average jerk vs. velocity for these three curves. This figure can be used as a design tool. The length of transition curve can be calculated using Eq. 2.4 when the velocity for a given degree of curvature is determined from the figure for a desired threshold average jerk. As an example, if the threshold jerk is defined as 2.5 ft/s^3 for a curve with 6th degree of curvature, the corresponding maximum velocity from Figure 4-16 is 17 mph. As a result, Eq. 2-4 results in a transition curve length of 170 ft.

As shown in the figure, average jerk for a 2nd order curve is less than the lower limit defined in AASHTO (2011). Hence, providing a transition curve length of 32 ft is adequate to maintain an average jerk of 1.0 ft/s^3 with a maximum bicycle velocity of 18 mph. Similarly, the results of 4th and 6th order curves can be used to calculate the length of transition curves for a defined maximum velocity. The findings presented here can be used for evaluating the comfort level of a cyclist when negotiating an existing curve. This is very useful when bicycle facilities are integrated into existing roadways. When the cyclist comfort as well as bicycle stability is a concern, other measures such as posting speed limits or warnings can be considered. Hence, using "SLOW DOWN" caution sign or street marking is suggested to post before the curve for warning a bicyclist to reduce the speed while negotiating a higher order horizontal curve to avoid loss of control as well as to increase the level of comfort.

Table 4-5. Average Jerk for Different Degrees of Curvature and Velocities Determined Through Simulations

Velocity (mph)	Averaged jerk (ft/s^3)		
	Degree of curvature		
	2nd	4th	6th
12.5	0.36	1.28	1.67
14.0	0.46	1.48	1.84
15.5	0.56	1.71	2.07
17.0	0.82	2.10	2.46
18.5	1.08	2.53	3.02

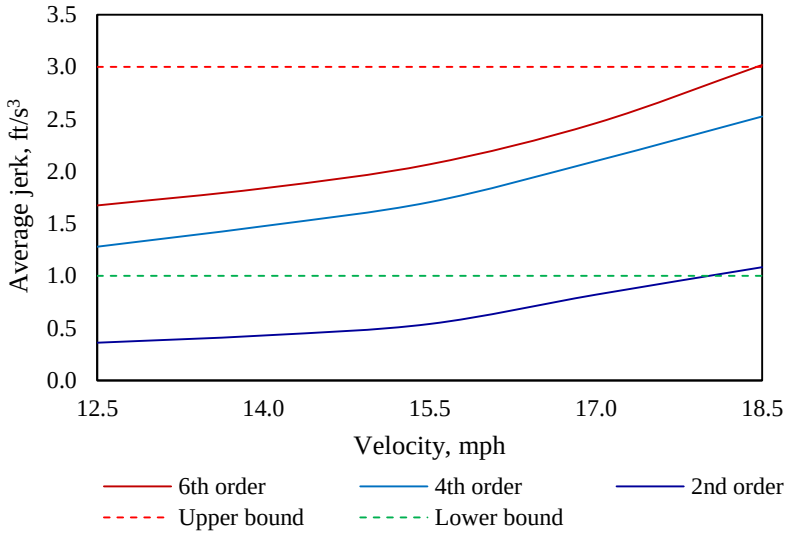

Figure 4-16. Average jerk vs. velocity

4.8 SUMMARY

A simulation model was developed in ADAMS environment, and is used to evaluate the impact of radius of a horizontal curve, transition curve, and velocity on stability and comfort of a cyclist. The model is simulated along a predefined route at 5 different velocities that are within the self-stable velocity region. Bicycle wheels are constrained during simulation to follow the curves using planar joints and point-to-curve contacts. Two schemes are adopted for assigning planar joint and point-to-curve contact. The front wheel is constrained with the curve in scheme 2 to evaluate the slip angle of the rear wheel while negotiating a curve. The slip angle increases with the increase of bicycle velocity and degree of curvature resulting in unstable conditions. Front and rear wheels are constrained to the curve in scheme 1 to evaluate the impact of centripetal acceleration on stability and ride comfort. Simulation results show a variation of centripetal acceleration at the entrance and exit of a curve as well as within a curve. Centripetal acceleration

increases with the increase of bicycle velocity and degree of curvature. Jerk is the change in acceleration. Hence, a sudden change in centripetal acceleration results in a higher jerk. The jerk is significant at the entrance and exit of a horizontal curve in the absence of properly designed transition curves. Cyclists feel discomfort and tend to lose control due to a sudden jerk. A graph showing the variation of average jerk vs. velocity is developed for different degrees of curvature. This graph can be used as a design tool for calculating the required length of transition curves or to evaluate the impact of existing curves on stability and comfort of a cyclist. When the available bicycle lane features cannot be altered to accommodate the required length of transition curves, due to existing roadway and space constraints, a “SLOW DOWN” caution sign or street marking is suggested to post before the curve to warn cyclists to avoid or minimize stability and ride comfort concerns.

5 SUMMARY, CONCLUSIONS, AND RECOMMENDATIONS

5.1 SUMMARY AND CONCLUSIONS

Cycling is regarded as an effective and efficient mode of transportation. Cycling is promoted as more emphasis is given to non-motorized mobility. To attract people towards cycling, safe and comfortable bikeways are needed while enhancing static and dynamic ride comfort and minimizing the excitations coming to the cycle-rider system. A bikeway facility is designed following the American Association of State Highway and Transportation officials (AASHTO) and the Highway Design Manual (HDM) specifications and guidelines. These manuals provide the minimum requirement of bikeway design parameters to develop a suitable human-cycling environment based on the speed limit and average annual daily traffic (AADT). Manufacturers are constantly working on various aspects of bicycle features and outfits to improve static and dynamic comfort of the rider. On the other hand, bikeway surface megatexture and roughness are improved using different material like cheap seals to improve ride comfort. Bikeway geometry also affects the comfort of cyclists. As an example, in the absence of transition curves, cyclists feel a jerk of varying magnitude at the entrance and exit of a horizontal curve. Experimental studies are conducted to improve safety and ride comfort. A majority of these studies are focused on reducing vertical excitation transmitted from the bikeway ride comfort. The other research focuses on the safety by evaluating the driver and cyclist responses and cyclist comfort while riding with the vehicles. The research methods implemented for such studies include verbal/written surveys, video recording, tracking bicycle positions using GPS devices and smartphones to evaluate the interaction of cyclists and the riding environment. In addition, instrumented bicycles and virtual reality are also used for such purposes. These methods are indispensable to evaluate human response and to understand the interaction. In addition to such efforts, simulation models can be used to evaluate the impact of several bikeway design parameters on stability (safety) and comfort.

A bicycle model is developed in ADAMS using Whipple benchmark model parameters to evaluate the impact of bikeway geometric design parameters on stability and comfort. The self-stable velocity region is established using the dynamic equation of motion and bicycle design parameters presented in Meijaard et al. (2007). The ADAMS bicycle model is validated using force equilibrium, theoretical centripetal acceleration, and experimental data obtained from an

instrumental probe bicycle (IPB). The validated bicycle model is simulated over a predefined bikeway at 5 different velocities. Bicycle movement along a predefined path is constrained by defining planar joint and point-to-curve contacts at the contact points of the wheels and the road. Two schemes of constraints are used for simulation. Scheme 1 includes planar joint and point-to-curve contacts at both wheels to evaluate jerk developed on the cyclist while travelling along a horizontal curve. Scheme 2 includes only one planar joint and point-to-curve contacts at the front wheel to evaluate the slip angle of the rear wheel due to degrees of curvature of the curves and velocity. The following conclusions are derived from this study:

- Slip angle increases with the increase in velocity and degree of curvature of a horizontal curve.
- ADAMS output shows variation of centripetal acceleration within a horizontal curve that results in a jerk.
- Jerk increases with the increase of degree of curvature and bicycle velocity.
- Jerk at the entrance and exit of a horizontal curve, in the absence of properly designed transition curves, is the highest along a route.
- A graph showing the variation of average jerk vs. velocity was developed for different degree of curvature. This graph can be used as a design tool for calculating the required length of transition curves or to evaluate the impact of existing curves on stability and comfort of a cyclist. When the available bicycle lane features cannot be altered to accommodate the required length of transition curves, due to existing roadway and space constraints, a “SLOW DOWN” caution sign or street marking is suggested to post before the curve to warn cyclists to avoid or minimize stability and ride comfort concerns.

5.2 RECOMMENDATIONS

The following implementation and future research recommendations are derived from this study:

- The simulation capabilities and the methodology presented in this report can be used to evaluate the impact of horizontal curve, velocity, and transition curves on bicycle stability and rider comfort.
- A graph is presented in this report that can be used as a design tool. This tool was developed by considering only one bicycle model and a weight of a single cyclist. This

tool needs to be further extended by incorporating various bicycle and rider characteristics to develop a tool that can be used to cover a wide range of such parameters during design of new bikeway and evaluation of existing bikeways or future implementations.

- The simulation model needs to be further improved by incorporating additional capabilities such as controlling lean and stability controls introduced by the cyclist.

6 REFERENCES

1. AASHTO (2011). "A Policy on Geometric Design of Highway and Streets." *American Association of State Highway and Transportation Officials (AASHTO)*, 444 North Capitol Street, NW, Suite 249, Washington DC 20001, USA.
2. AASHTO (2012). "Guide for the Development of Bicycle Facility." *American Association of State Highway and Transportation Officials (AASHTO)*, 444 North Capitol Street, NW, Suite 249, Washington DC 20001, USA.
3. ADDO INDIA (2018). <http://www.eastmanautotyres.com/otr-technology.html> (Last visited August 20, 2018).
4. Åström, K. J., Klein, R. E., and Lennartsson, A. (2005). "Bicycle Dynamics and Control, Adapted Bicycles for Education and Research." *IEEE Control System Magazine*, Volume 25, pg. 26–47. (doi:10.1109/MCS.2005.1499389)
5. Attanayake, U., Mazumder, A. F., Sahi, W. D., Mueller, M., and Black, D. (2017). "Enhancing Non-Motorized Mobility within Construction Zones." *Report to the TRC-LC, Western Michigan University (WMU)*, 1903 W Michigan Ave, Kalamazoo, Michigan 49008, USA.
6. Basu-Mandal, P., Chatterjee, A., and Papadopoulos, J. M. (2007). "Hands-Free Circular Motions of a Benchmark Bicycle." *Proceedings of the Royal Society A: Mathematical, Physical and Engineering Sciences*, 463(March), 1983–2003.
7. BDE Manual (2016). "Bureau of Design and Environment Manual-Chapter 17: Policy & Procedures Section." *Illinois Department of Transportation (IDOT)*, 2300 South Dirksen Parkway, Room No. 330 Springfield, Illinois 62764, USA.
8. Bicycling (2018). "How to Achieve the Perfect Bike Tire Pressure." <https://www.bicycling.com/repair/a20004232/how-to-achieve-the-perfect-bike-tire-pressure/> (Last Accessed August 20, 2018)
9. Caltrans HDM (2016). "California Highway Design Manual." *California Department of Transportation (Caltrans DOT)*, 1120 N Street, Sacramento, California 95814, USA.
10. Cain, S. M. and Perkins, N. C. (2010). "Comparison of a Bicycle Steady-State Turning Model to Experimental Data." *Bicycle and Motorcycle Dynamics Symposium*, Dynamics and Control of Single Track Vehicles, Delft, Netherlands.

11. Cervélo (2015). “Ride Quality.” <https://www.cervelo.com/en/Engineering-Field-Notes/Engineering-Fundamentals/Ride-Quality> (Last Accessed August 20, 2018).
12. Chen, P., Shen, Q., and Childress, S. (2018). “A GPS Data-Based Analysis of Built Environment Influences on Bicyclists Route Preferences.” *International Journal of Sustainable Transportation*, Volume 12, No, 3, pg. 218–231.
13. Cheng, K. Y., Bothman, D., and Åström, K. J. (2003). “Bicycle Torque Sensor Experiment.” Technical Report, *University of California – Santa Barbara*, Santa Barbara, CA 93106, USA.
14. Connors, B. (2009). “Modeling and Stability Analysis of a Recumbent Bicycle with Oscillating Leg Masses.” M.Sc. Thesis, *University of California – Davis*, 1 Shields Ave, Davis, CA 95616, USA.
15. Cycling Weekly (2018). “10 Best Ways to Make Your Bike More Comfortable.” <https://www.cyclingweekly.com/news/latest-news/10-best-ways-to-make-your-bike-more-comfortable-205074> (Last Accessed August 20, 2018).
16. CYCLINGTIPS (2018). “The Beauty of Cycling.” <https://cyclingtips.com/2016/06/the-science-of-bike-building-what-factors-affect-ride-quality-and-what-even-is-it/> (Last Accessed August 20, 2018).
17. De Leeuw, G. and De Kruijf, J. (2015). “The Act of (Future) Cycling: Testing Urban Designs and Conducting Research in Virtual Reality.” *European Transport Conference*, Association of European Transport, Frankfurt, Germany, pg. 1-15.
18. Dikarev, E. D., Dikareva, S. B., and Fufaev, N. A. (1981). “Effect of Inclination of Steering Axis and of Stagger of the Front Wheel on Stability of Motion of a Bicycle.” *Izv. Akad. Nauk SSSR Mekh. Tverd. Tela* 16, 69–73. [Translated by Mechanics of Solids, Volume 16, pg. 60–63]
19. IRC (2010). “Two-lane of Highway Through Public Private Partnership: Manual of Specifications & Standards”, *Planning Commission Government of India*, The Indian Road Congress (IRC), Sector 6, R. K. Puram, New Delhi 110 022, India.
20. Johnson, M., Charlton, J., Oxley, J., and Newstead, S. (2010). “Naturalistic Cycling Study: Identifying Risk Factors for On-Road Commuter Cyclists.” *Annals of Advances in Automotive Medicine*, Vol. 54, pp. 275–283.

21. Kane, T. R. (1968). "Dynamics." *NY: Holt, Rinehart and Winston*, New York, USA.
22. Kostich, B. W. (2017). "Development of Empirical and Virtual Tools for the Study of Bicycle Safety." MSc. Thesis, *Western Michigan University*, Michigan, USA.
23. Lépine, J., Champoux, Y., and Droet, J. -M. (2013). "A Laboratory Excitation Technique to Test Road Bike Vibration." Experimental Techniques, *Society for Experimental Mechanics*, pg. 1-8.
24. Li, H., Harvey, J. T., Thigpen, C., and Wu, R. (2014). "Surface Treatment Macrotexture and Bicycle Ride Quality." Research Report: UCPRC-RR-2013-07, *California Department of Transportation (Caltrans)*, 1120 N Street, Sacramento, California 94273, USA.
25. Limebeer, D. J. N. and Sharp, R. S. (2006). "Bicycles, Motorcycles, and Models." *IEEE Control Systems Magazine*, Volume 26, pg. 34–61.
26. Lorenzo, D. S. D. (1997). "Quantification of Structural Loading during Off-Road Cycling." M.Sc. Thesis, *University of California – Davis*, 1 Shields Ave, Davis, CA 95616, USA.
27. Maleque, M. A. and Dyuti, S. (2010). "Material Selection of a Bicycle Frame Using Cost Per Unit Property and Digital Logic Methods." *International Journal of Mechanical and Materials Engineering (IJMME)*, Volume 5, No. 1, pg. 95-100.
28. Mears, B. C. (1988). "Open Loop Aspects of Two Wheeled Vehicle Stability Characteristics." Ph.D. Thesis, *University of Illinois at Urbana-Champaign*, Illinois, USA.
29. Meijaard, J. P. (2004). "Derivation of the Linearized Equations for an Uncontrolled Bicycle. Internal Report, *University of Nottingham*, United Kingdom.
30. Meijaard, J. P., Papadopoulos, J. M., Ruina, A., and Schwab, A. L. (2007). "Linearized Dynamics Equations for the Balance and Steer of a Bicycle: A Benchmark and Review." *Proceedings of the Royal Society A: Mathematical, Physical and Engineering Sciences*, 463, pg. 1955–1982.
31. MnDOT (2007). "Bikeway Facility Design Manual." *Minnesota Department of Transportation (MnDOT)*, 222 Plato Blvd E, St Paul, MN 55107, USA.
32. Moore, J. K. (2012). "Human Control of a Bicycle." Ph.D. dissertation, *University of California-Davis*, CA 95616, USA.
33. NACTO (2018). "Urban Bikeway Design Guide." *National Association of City Transportation Officials*, 120 Park Avenue 20th Floor, New York 10017, USA.

<https://nacto.org/publication/urban-bikeway-design-guide/bike-lanes/> (Last Accessed August 20, 2018).

34. NAPA (2002). "A Guideline for the Design and Construction of HMA Pavements for Trails and Paths." *National Asphalt Pavement Association*, 5100 Forbes Boulevard, Lanham, Maryland 20706, USA.
35. NCHRP (2014). "Recommended Bicycle Lane Widths for Various Roadway Characteristics." *National Cooperative Highway Research Program*, Transportation Research Board, 500 Fifth Street, NW, Washington DC 20001, USA.
36. NCM (2011). "National Cycle Manual." *National Transport Authority*, Dún Scéine, Harcourt Lane, Dublin 2, Ireland.
37. Oh, J. S., Kwigizile, V., Ro, K., Feizi, A., Kostich, B. W., Hasan, R. A. H., and Alhomaidat, F. A. M. (2017). "Effect of Cycling Skills on Bicycle Safety and Comfort Associated with Bicycle Infrastructure and Environment." *Report to the TRC-LC, Western Michigan University (WMU)*, 1903 W Michigan Ave, Kalamazoo, Michigan 49008, USA.
38. Papadopoulos, J. M. (1987). "Bicycle Steering Dynamics and Self-Stability: A Summary Report on Work in Progress." Technical Report, *Cornell Bicycle Research Project, Cornell University*, NY 14853, USA.
39. Papadopoulos, J. M. (1988). "Bicycle Dynamics – The Meaning Behind the Math." *Bike Tech*, pg. 13-15.
40. Peterson, D. L. and Hubbard, M. (2009). "General steady turning of a benchmark bicycle model." In Proceedings of IDETC/MSNDC, *International Design Engineering Technical Conferences & 7th International Conference on Multibody Systems*, Nonlinear Dynamics, and Control, number DETC2009/MSNDC-86145.
41. Sharp, R. S. (2007). "Optimal Stabilization and Path-Following Controls for a Bicycle." Proceeding of the Institute of Mechanical Engineers – Part C, *Journal of Mechanical Engineering Science*, Volume 221. No. (4), pg. 415 – 427.
42. Sharp, R. S. (2008). "On the Stability and Control of the Bicycle." *Applied Mechanics Review*, Volume 61 (6): 24.
43. Smart Growth America (2013). "Complete Street Policies: Legal Workbook." *Smart Growth America*, 1707 L St NW Suite, 250 Washington DC 20036, USA.

44. Statista (2018). "Number of Cyclists/Bike Rider within the Last 12 Months in the United States from Spring 2008 to Spring 2017 (in millions)." <http://www.statista.com/statistics/227415/number-of-cyclists-and-bike-riders-usa/> (Last Accessed August 20, 2018)
45. Strogatz, S. H. (1994). "Non-linear Dynamics and Chaos: with Applications to Physics, Biology, Chemistry, and Engineering." *Perseus Books*, Cambridge, UK
46. The Constructor (2018). <https://theconstructor.org/transportation/horizontal-transition-curves-highways/11271/> (Last Accessed August 20, 2018).
47. Thigpen, C. G., Li, H., and Harvey, J. (2015). "Modeling the Impact of Pavement Roughness on Bicycle Ride Quality." *Transportation Research Board (TRB)*, 500 Fifth St NW, Washington D.C 20001, USA.
48. VÉLUS (2018). <http://velus.recherche.usherbrooke.ca/index.html> (Last Accessed August 20, 2018).
49. Whipple, F. J. W. (1899). "The Stability of the Motion of a Bicycle." The Quarterly Journal of Pure and Applied Mathematics, Volume 30, pg. 312–348.
50. Wikipedia (2018). <https://en.wikipedia.org/wiki/List_of_bicycle_parts> (Last Accessed August 20, 2018).
51. Wikstrom, M. (2016). "The Science of Bike Building: What is 'Ride Quality' and What Factors Affect it?" <https://cyclingtips.com/2016/06/the-science-of-bike-building-what-factors-affect-ride-quality-and-what-even-is-it/> (Last Accessed July 7, 2018).
52. Yeboah, G. and Alvanides, S. (2015). "Route Choice Analysis of Urban Cycling Behaviors Using OpenStreetMap: Evidence from a British Urban Environment." *Springer International Publishing Switzerland AG*, Cham Switzerland, pg. 189-210, ISBN 978-3-319-14279-1.

APPENDIX A: ABBREVIATION

A

AADT	Average Annual Daily Traffic
AASHTO	American Association of State Highway and Transportation Officials
ADAMS	Automatic Dynamic Analysis of Mechanical Systems

C

Caltrans	California Department of Transportation
CG	Centre of Gravity
CFRP	Carbon Fiber Reinforced Polymer

D

DOT	Department of Transportation

F

FPS	Foot Pound Second

G

GFRP	Glass Fiber Reinforced Polymer

I

IPB	Instrumented Probe Bicycle

K

KFRP	Kevlar Fiber Reinforced Polymer

M

MKS	Meter Kilogram Second

N

NACTO	National Association of City Transportation Officials
NCM	National Cycle Manual

U

USA	United States of America

APPENDIX B: COEFFICIENTS OF LINEARIZED EQUATIONS

The coefficients of the linearized equation (Meijaard et al. 2007) are calculated using the formulae presented below. All the equations are derived with respect to the rear contact point P.

The total mass and the corresponding center of mass

$$m_T = m_R + m_B + m_H + m_F \quad \text{(B 1)}$$

$$x_T = \left(\frac{x_B m_B + x_H m_H + w m_F}{m_T}\right) \quad \text{(B 2)}$$

$$z_T = \left(\frac{-r_R m_R + z_B m_B + z_H m_H - r_F m_F}{m_T}\right) \quad \text{(B 3)}$$

Relevant mass moments and products of inertia

$$I_{Txx} = I_{Rxx} + I_{Bxx} + I_{Hxx} + I_{Fxx} + m_R r_R^2 + m_B z_B^2 + m_H z_H^2 + m_F r_F^2 \quad \text{(B 4)}$$

$$I_{Txz} = I_{Bxz} + I_{Hxz} - m_B x_B z_B + m_H x_H z_H + m_F w r_F \quad \text{(B 5)}$$

$$I_{Rzz} = I_{Rxx},\ I_{Fzz} = I_{Fxx}, \quad \text{(B 6)}$$

$$I_{Tzz} = I_{Rzz} + I_{Bzz} + I_{Hzz} + I_{Fzz} + m_B x_B^2 + m_H x_H^2 + m_F w^2 \quad \text{(B 7)}$$

Total mass, center of mass, and mass moment of inertias for front assembly

$$m_A = m_H + m_F \quad \text{(B 8)}$$

$$x_A = \left(\frac{x_H m_H + w m_F}{m_A}\right), z_A = \left(\frac{z_H m_H - r_F m_F}{m_A}\right) \quad \text{(B 9)}$$

$$I_{Axx} = I_{Hxx} + I_{Fxx} + m_H (z_H - z_A)^2 + m_F (r_F + z_A)^2 \quad \text{(B 10)}$$

$$I_{Axz} = I_{Hxz} - m_H (x_H - x_A)(z_H - z_A) + m_F (w - x_A)(r_F + z_A) \quad \text{(B 11)}$$

$$I_{Azz} = I_{Hzz} + I_{Fzz} + m_H (x_H - x_A)^2 + m_F (w - x_A)^2 \quad \text{(B 12)}$$

The perpendicular distance from the center of mass of front assembly to the steering axis

$$u_A = (x_A - w - c)\cos\lambda - z_a \sin\lambda \quad \text{(B 13)}$$

The moment of inertia about steer axis and the product of inertia relative to crossed, skew axes

$$I_{A\lambda\lambda} = m_A u_A^2 + I_{Axx} \sin^2\lambda + 2 I_{Axz} \sin\lambda \cos\lambda + I_{Azz} \cos^2\lambda \quad \text{(B 14)}$$

$$I_{A\lambda x} = -m_A u_A z_A + I_{Axx} \sin\lambda + I_{Axz} \cos\lambda \quad \text{(B 15)}$$

$$I_{A\lambda z} = m_A u_A x_A + I_{Axz} \sin\lambda + I_{Azz} \cos\lambda \quad \text{(B 16)}$$

The ratio of mechanical trail

$$\mu = \left(\frac{c}{w}\right)\cos\lambda \quad \text{(B 17)}$$

The gyrostatic coefficients

$$S_R = \frac{I_{Ryy}}{r_R},\ S_F = \frac{I_{Fyy}}{r_F},\ S_T = S_R + S_F \quad \text{(B 18)}$$

$$S_A = m_A u_A + \mu m_T x_T \quad \text{(B 19)}$$

Mass moments of inertia

$$M = \begin{bmatrix} M_{\phi\phi} & M_{\phi\delta} \\ M_{\delta\phi} & M_{\delta\delta} \end{bmatrix} \quad \text{(B 20)}$$

$$M = \begin{bmatrix} I_{Txx} & I_{A\lambda x} + \mu I_{Txz} \\ I_{A\lambda x} + \mu I_{Txz} & I_{A\lambda\lambda} + 2\mu I_{A\lambda z} + \mu^2 I_{Tzz} \end{bmatrix} \quad \text{(B 21)}$$

The gravity-dependent stiffness matrix

$$K_o = \begin{bmatrix} K_{o\phi\phi} & K_{o\phi\delta} \\ K_{o\delta\phi} & K_{o\delta\delta} \end{bmatrix} \tag{B 22}$$

$$K_o = \begin{bmatrix} m_T z_T & -S_A \\ -S_A & -S_A \sin\lambda \end{bmatrix} \tag{B 23}$$

The velocity-dependent stiffness matrix

$$K_2 = \begin{bmatrix} K_{2\phi\phi} & K_{2\phi\delta} \\ K_{2\delta\phi} & K_{2\delta\delta} \end{bmatrix} \tag{B 24}$$

$$K_2 = \begin{bmatrix} 0 & \left(\frac{S_T - m_T z_T}{w}\right)\cos\lambda \\ 0 & \left(\frac{S_A + S_F \sin\lambda}{w}\right)\cos\lambda \end{bmatrix} \tag{B 25}$$

The damping matrix

$$C_1 = \begin{bmatrix} C_{1\phi\phi} & C_{1\phi\delta} \\ C_{1\delta\phi} & C_{1\delta\delta} \end{bmatrix} \tag{B 26}$$

$$C_1 = \begin{bmatrix} 0 & \mu S_T + S_F \cos\lambda + \left(\frac{I_{Txz}}{w}\right)\cos\lambda - \mu m_T z_T \\ -(\mu S_T + S_F \cos\lambda) & \left(\frac{I_{A\lambda z}}{w}\right)\cos\lambda + \mu\left(S_A + \left(\frac{I_{Tzz}}{w}\right)\cos\lambda\right) \end{bmatrix} \tag{B 27}$$

APPENDIX C: MATLAB CODE

```
% This code is developed by Abul Fazal Mazumder
% A Ph.D. student of Western Michigan University
clc;
clear all;
close all;
%% Input parameters
w=1.02;          % Wheel base (m)
c=0.08;          % Trail (m)
lamda=pi/10;     % Steer axis tilt (rad)
g=9.81;          % Gravitational acceleration (N/kg or m/s)
%v=zeros(100,1);% Forward velocity of bicycle (m/s)

% Rear wheel, R
rR=0.3;          % Radius (m)
mR=2;            % Mass (kg)
IRxx=0.0603;     % Mass moments of inertia (kg m^2)
IRyy=0.0603;     % Mass moments of inertia (kg m^2)

% Read body and frame assembly, B
xB=0.3;          % Position of center of mass (m)
zB=-0.9;         % Position of center of mass (m)
mB=85;           % Mass (kg)
IBxx=9.2;        % Mass moment of inertia (kg m^2)
IByy=11;         % Mass moment of inertia (kg m^2)
IBzz=2.8;        % Mass moment of inertia (kg m^2)
IBxz=0;          % Mass moment of inertia (kg m^2)

% Front handlebar and fork assembly, H
xH=0.91;         % Position of center of mass (m)
zH=-0.68;        % Position of center of mass (m)
mH=4;            % Mass (kg)
IHxx=0.05892;    % Mass moment of inertia (kg m^2)
IHyy=0.12;       % Mass moment of inertia (kg m^2)
IHzz=0.00708;    % Mass moment of inertia (kg m^2)
IHxz=0;          % Mass moment of inertia (kg m^2)

% Front wheel, F
rF=0.35;         % Radius (m)
mF=3;            % Mass (kg)
IFxx=0.1405;     % Mass moments of inertia (kg m^2)
IFyy=0.1405;     % Mass moments of inertia (kg m^2)
%% Calculation
%% Total mass and center of mass location with respect to rear contact point
P
mT=mR+mB+mH+mF;                                                  % B 1
xT=(xB*mB+xH*mH+w*mF)/mT;                                        % B 2
zT=(-rR*mR+zB*mB+zH*mH-rF*mF)/mT;                                % B 3
%% Relevant mass moments and products of inertia with respect to rear contact
point P
ITxx=IRxx+IBxx+IHxx+IFxx+mR*rR^2+mB*zB^2+mH*zH^2+mF*rF^2;        % B 4
ITxz=IBxz+IHxz-mB*xB*zB-mH*xH*zH+mF*w*rF;                        % B 5
IRzz=IRxx; IFzz=IFxx;                                            % B 6
ITzz=IRzz+IBzz+IHzz+IFzz+mB*xB^2+mH*xH^2+mF*w^2;                 % B 7
%% Total mass, center of location, and mass moment of inertia with respect to
rear contact point P
mA=mH+mF;                                                        % B 8
xA=(xH*mH+w*mF)/mA; zA=(zH*mH-rF*mF)/mA;                         % B 9
```

```
IAxx=IHxx+IFxx+mH*(zH-zA)^2+mF*(rF+zA)^2;                          % B 10
IAxz=IHxz-mH*(xH-xA)*(zH-zA)+mF*(w-xA)*(rF+zA);                    % B 11
IAzz=IHzz+IFzz+mH*(xH-xA)^2+mF*(w-xA)^2;                          % B 12
%% The center of mass of the front assembly form the center of mass of front
wheel
uA=(xA-w-c)*cos(lamda)-zA*sin(lamda);                              % B 13
%% Three special inertia quantities
IAll=mA*uA^2+IAxx*(sin(lamda))^2+2*IAxz*sin(lamda)*cos(lamda)+IAzz*(cos(lamda
))^2;  % A 14
IAlx=-mA*uA*zA+IAxx*sin(lamda)+IAxz*cos(lamda);                    % B 15
IAlz=mA*uA*xA+IAxz*sin(lamda)+IAzz*cos(lamda);                     % B 16
%% The ratio of mechanical trail
nu=(c/w)*cos(lamda);                                               % B 17
%% Gyroscopic coefficients
SR=IRyy/rR; SF=IFyy/rF; ST=SR+SF;                                  % B 18
SA=mA*uA+nu*mT*xT;                                                 % B 19
%% Mass Matrix, M
M=zeros(2,2);
M(1,1)=ITxx; M(1,2)=IAlx+nu*ITxz; M(2,1)=M(1,2);
M(2,2)=IAll+2*nu*IAlz+nu^2*ITzz;   % A 20
M;                                                                 % B 21
%% Gravity-dependent stiffness matrix, Ko
Ko=zeros(2,2);
Ko(1,1)=mT*zT; Ko(1,2)=-SA; Ko(2,1)=Ko(1,2); Ko(2,2)=-SA*sin(lamda);  % B 22
Ko;                                                                % B 23
%% Velocity-dependent stiffness matrix, K2
K2=zeros(2,2);
K2(1,1)=0; K2(1,2)=((ST-mT*zT)/w)*cos(lamda); K2(2,1)=0;
K2(2,2)=((SA+SF*sin(lamda))/w)*cos(lamda);    % A 24
K2;                                                                % B 25
%% Damping-like matrix, C
C=zeros(2,2);
C(1,1)=0; C(1,2)=nu*ST+SF*cos(lamda)+(ITxz/w)*cos(lamda)-nu*mT*zT;
C(2,1)=-(nu*ST+SF*cos(lamda));
C(2,2)=(IAlz/w)*cos(lamda)+nu*(SA+(ITzz/w)*cos(lamda));             % B 26
C;                                                                 % B 27
%% Finding eigenvalues
syms v; syms sigma;
EOM=M*sigma^2+v*C*sigma+g*Ko+v^2*K2;
vpa(EOM);
d=det(EOM);
vpa(d);
s=vpa(solve(d,sigma),4);

vel=zeros(100,1);
sol=zeros(100,4);
for i=1:100
    vel(i,1)=i/10;
    aa=vpa(subs(s,v,i/10),15);
    sol(i,:)=aa(:,1);
end

plot(vel,sol)
```